

Article

Cadmium Highlights Common and Specific Responses of Two Freshwater Sentinel Species, *Dreissena polymorpha* and *Dreissena rostriformis bugensis*

Florence Bultelle ^{1,*}, Aimie Le Saux ¹ , Elise David ² , Arnaud Tanguy ³ , Simon Devin ⁴, Stéphanie Olivier ¹, Agnès Poret ¹, Philippe Chan ^{5,6}, Fanny Louis ^{2,4}, Laurence Delahaut ², Sandrine Pain-Devin ⁴, Romain Péden ² , David Vaudry ⁷, Frank Le Foll ¹ and Béatrice Rocher ¹

¹ UMR-I 02 INERIS-SEBIO, UFR ST, Scale FR-CNRS 3730, Le Havre Normandie University, 76063 Le Havre, France; beatrice.rocher@univ-lehavre.fr (B.R.)

² UMR-I 02 INERIS-SEBIO, UFR SEN, Reims Champagne-Ardenne University, 51100 Reims, France; elise.david@univ-reims.fr (E.D.)

³ UMR 7144, CNRS, Station Biologique de Roscoff, Sorbonne University, 29680 Roscoff, France; atanguy@sb-roscoff.fr

⁴ LIEC, CNRS, UFR SCIFA, Lorraine University, 57000 Metz, France; simon.devin@univ-lorraine.fr (S.D.)

⁵ INSERM US 51, CNRS UAR 2026, HeRaLeS, Rouen Normandie University, 76821 Mont-Saint-Aignan, France

⁶ PISSARO IRIB, Rouen Normandie University, 76821 Mont-Saint-Aignan, France

⁷ INSERM U982 DC2N, Rouen Normandie University, 76821 Mont-Saint-Aignan, France

* Correspondence: florence.bultelle@univ-lehavre.fr

Abstract: Zebra mussel (ZM), *Dreissena polymorpha*, commonly used as a sentinel species in freshwater biomonitoring, is now in competition for habitat with quagga mussel (QM), *Dreissena rostriformis bugensis*. This raises the question of the quagga mussel's use in environmental survey. To better characterise QM response to stress compared with ZM, both species were exposed to cadmium ($100 \mu\text{g}\cdot\text{L}^{-1}$), a classic pollutant, for 7 days under controlled conditions. The gill proteomes were analysed using two-dimensional electrophoresis coupled with mass spectrometry. For ZM, 81 out of 88 proteoforms of variable abundance were identified using mass spectrometry, and for QM, 105 out of 134. Interestingly, the proteomic response amplitude varied drastically, with 5.6% of proteoforms of variable abundance (DAPs) in ZM versus 9.4% in QM. QM also exhibited greater cadmium accumulation. Only 12 common DAPs were observed. Several short proteoforms were detected, suggesting proteolysis. Functional analysis is consistent with the pleiotropic effects of the toxic metal ion cadmium, with alterations in sulphur and glutathione metabolisms, cellular calcium signalling, cytoskeletal dynamics, energy production, chaperone activation, and membrane events with numerous proteins involved in trafficking and endocytosis/exocytosis processes. Beyond common responses, the sister species display distinct reactions, with cellular response to stress being the main category involved in ZM as opposed to calcium and cytoskeleton alterations in QM. Moreover, QM exhibited greater evidence of proteolysis and cell death. Overall, these results suggest that QM has a weaker stress response capacity than ZM.

Keywords: quagga mussel; zebra mussel; proteoforms; stress; biomonitoring



Citation: Bultelle, F.; Le Saux, A.; David, E.; Tanguy, A.; Devin, S.; Olivier, S.; Poret, A.; Chan, P.; Louis, F.; Delahaut, L.; et al. Cadmium Highlights Common and Specific Responses of Two Freshwater Sentinel Species, *Dreissena polymorpha* and *Dreissena rostriformis bugensis*. *Proteomes* **2024**, *12*, 10. <https://doi.org/10.3390/proteomes12020010>

Academic Editors: Matthew P. Padula and Jens R. Coorssen

Received: 8 November 2023

Revised: 20 February 2024

Accepted: 18 March 2024

Published: 26 March 2024



Copyright: © 2024 by the authors. Licensee MDPI, Basel, Switzerland. This article is an open access article distributed under the terms and conditions of the Creative Commons Attribution (CC BY) license (<https://creativecommons.org/licenses/by/4.0/>).

1. Introduction

Aquatic environments are subject to extensive perturbations caused by abiotic factors such as temperature or oxygen levels and pollution. Assessing ecosystem health is crucial to understanding the impact of human activity and enhancing the preservation and remediation of natural habitats. In the European Union, this necessity, first underlined by the scientific community, has been reinforced by legally binding directives aimed at improving water quality. The Water Framework Directive (2013/39/EC) introduced new environmental quality standards for priority substances and certain other pollutants. It

also set 2027 as the target date for achieving good status for water bodies. Currently, the definition of “good status” is based on chemical and ecological data but does not include an assessment of the health of biota via ecotoxicological data. A European Consortium was established to enhance regulations by utilising innovative biological monitoring techniques. The consortium recommends the development of integrated effect-based methods for environmental survey. To this end, it is crucial to identify the mechanisms and molecular players involved in the stress response of the species under consideration.

Sentinel or bioindicator species are chosen to represent the biota in biomonitoring studies. The species selected must meet certain biological and ecological criteria, such as being representative of its environment and of the collection site, having the capacity to bioaccumulate pollutants over time and having a wide distribution area. Technical criteria are also considered, i.e., ease of identification and year-round availability for collection. In coastal and marine environments, *Mytilus* species are the most widely used. They are sedentary filter-feeders and have a good capacity to bioaccumulate pollutants, combined with a low capacity for biotransformation. Zebra mussel (ZM), *Dreissena polymorpha* (Pallas, 1771) is a very similar biological model that closely resembles *Mytilus* and has been used as a counterpart in freshwater ecosystems since the 1970s [1]. ZM are sedentary filter-feeding organisms with high filtration activity; they bioaccumulate many contaminants. They originate from the Ponto–Caspian area and have largely colonised Western Europe and also North America, especially the Great Lakes region [2]. More recently, the quagga mussel (QM), *Dreissena rostriformis bugensis* (Andrusov, 1897), a closely related dreissenid also native to the Ponto–Caspian region, has in turn become invasive in Western Europe and North America [3]. The coexistence of the two species within the same area and the QM’s displacement of ZM in some locations raises the question of using the QM as a counterpart sentinel species.

In 2022, Karatayev and Burlakova reviewed the existing knowledge on these two dreissenids [4]. In brief, ZM and QM exhibit physiological differences including variances in temperature and salinity tolerances, byssal thread attachment, growth rate, respiration rate, assimilation efficiency, and reproductive outcomes. Although QM has been found to be less tolerant of high temperatures than ZM, it withstands low temperatures better. Additionally, QM features a higher filtration rate but a lower respiration rate relative to ZM. Differential xenobiotic accumulation has been observed in both species in biomonitoring studies. For instance, Schäfer and collaborators reported that QM accumulated more organochlorine pesticides, experienced greater DNA damage, and exhibited lower levels of HSP stress proteins compared to ZM [5]. In contrast, Kerambrun and collaborators recorded a higher bioaccumulation of metals (Cd, Cu, Ni, Pb and Zn) and a higher gene expression level of the antioxidant enzyme catalase in ZM than in QM during a field study at a site shared by both species [6]. In a comparison of haemocyte oxidative activity, QM was shown to have a higher level of ROS than ZM [7]. Differences in biomarker responses were also noted between the two species after controlled metal exposure [8,9]. Energy allocation and antioxidant capacity varied between QM and ZM, wherein QM displayed more cellular damage upon cadmium exposure [8]. However, Farkas et al. (2017) observed no interspecies variation when comparing the responses of different biomarkers (such as EROD activity, lipid peroxidation, DNA damage, metallothionein, and vitellogenin) in ZM and QM populations from contaminated sites in Hungary [10]. Therefore, the above-mentioned disparities impede the mere transfer of biomarkers developed in ZM to QM and emphasise the necessity of further characterising contaminant effects on QM.

In this study, in order to compare the biological responses of the two species, we exposed QM and ZM to a single model toxicant under identical, controlled conditions. Cadmium was selected due to its well-known effects and high toxicity. Furthermore, cadmium is one of the four priority metals of the Water Framework Directive and is widely distributed in the aquatic environment [11]. Environmental cadmium concentrations in water can occasionally reach very high levels, such as 40 $\mu\text{g}\cdot\text{L}^{-1}$ in the Longjiang and Liujiang rivers in China [12] and 100 $\mu\text{g}\cdot\text{L}^{-1}$ in the water of the upper Malwathu Oya in

Sri Lanka [13]. Here, proteomic comparisons were conducted on gills, a tissue involved in respiration, feeding, ion regulation, and excretion of metabolic products. Cadmium can be absorbed through the digestive tract in aquatic organisms, but part of its internalisation also occurs in permeable areas like gills, where cadmium borrows from metal or calcium membrane transporters.

The aim of this study was to improve the understanding of (i) *Dreissena* species and (ii) the sensitivity and responses of *Dreissena polymorpha* and *Dreissena rostriformis bugensis* in a biomonitoring perspective. By exploring the proteomic level, the mechanistic basis of the different ecophysiological profiles can be evidenced. Mussels from both species were exposed to cadmium at a high but realistic concentration of $100 \mu\text{g}\cdot\text{L}^{-1}$ for 7 days. Two-dimensional electrophoresis was performed to investigate the differential expression profile of gill proteins. Variant proteoforms were identified by means of mass spectrometry using species-specific transcriptomic data, and then classified into functional categories. Some of these functional categories are common to both species, pointing to a shared response to heavy metal, whereas others are unique to each species, offering new insight into the species-specific aspects of the response to cadmium.

2. Materials and Methods

2.1. Organism Collection

Mussels were hand collected in February 2017. ZM were collected in the Meuse channel (Euville, France, N $48^{\circ}44'03''$, E $05^{\circ}39'45''$) and QM in the Saône river (Seurre, France, N $47^{\circ}00'03''$, E $05^{\circ}08'34''$). Individuals of both species were retrieved by section of the byssal thread. Mussels were quickly brought to the laboratory in aerated field water and mussel shells were gently cleaned to remove any organic deposits. Water physico-chemical parameters were measured onsite at the time of sampling. Cadmium concentrations were measured in samples of water with flameless atomic absorption spectrometry using SpectrAA 220 Zeeman (Varian, Mulgrav, The Netherlands) and revealed no cadmium contamination at both sites [14].

2.2. Acclimation

Mussels were grouped per species in tanks containing aerated field water at field temperature. During the first three days, water was gradually replaced by spring water (Cristaline[®], Aurèle spring, Alma, Jandun, France). Acclimation continued for 21 days in aerated water maintained at field temperature. An artificial photoperiod was applied based on natural conditions. During this period, water was totally renewed twice a week, and mussels were fed with a fresh diet of *Chlorella* and *Senedesmus* (Greensea) at the rate of 106 cells/individual/day. Water physico-chemical parameters, checked daily, were stable (temperature 4.8°C ; pH 8.2).

2.3. Exposure Design and Tissue Sampling

After 21 days of acclimation, for each species, mussels from the different tanks were pooled and separated again in order to define 2 experimental conditions: 7 days of cadmium exposure and control. A stock solution of CdCl_2 at $1 \text{ mg}\cdot\text{L}^{-1}$ acidified with 0.3% nitric acid was used and diluted to a final concentration of $100 \mu\text{g}\cdot\text{L}^{-1}$ in media. Meanwhile, control mussels were kept in spring water (Cristaline[®], Aurèle spring). The animals were maintained in aerated water at field temperature, and subjected to an artificial photoperiod consistent with the acclimation condition. Every day, water was renewed (control and exposed media) and mussels were fed according to the rate used during the acclimation phase. Water parameters were monitored daily. During the experiment, temperature, pH, and conductivity did not change between groups and no mortality was observed (Figure S1).

Water Cd concentrations were measured twice a day, immediately prior to the renewal and 2 h later. Actual water Cd concentrations reached $52.8 \pm 2.1 \mu\text{g}\cdot\text{L}^{-1}$ 2 h after the renewal and decreased to $14.7 \pm 3.1 \mu\text{g}\cdot\text{L}^{-1}$ within the 24 h for ZM and $41.4 \pm 3.8 \mu\text{g}\cdot\text{L}^{-1}$ to $6.9 \pm 0.1 \mu\text{g}\cdot\text{L}^{-1}$ for QM. After 7 days, cadmium accumulation was measured in mussels

($n = 12$). Soft tissues were dried at 60 °C for 24 h and digested in nitric acid 65% for 48 h at 80 °C. Metal quantifications were performed in the resulting acid solutions (adjusted to 3 mL with deionised water) using flameless atomic absorption spectroscopy, as described in Amiard et al. [14]. Results are expressed in $\mu\text{g}\cdot\text{g}^{-1}$ of dry weight. For 2DE analysis, the gills of 12 mussels were sampled for each group: control zebra mussels (ZM-control), exposed zebra mussels (ZM-Cd), control quagga mussels (QM-control), and exposed quagga mussels (QM-Cd). The tissues were dissected, flash-frozen in liquid nitrogen and stored at -80 °C until analysis. Mussels were measured and weighted at the time of the sampling and no difference in the condition index was observed between exposed and treated groups for both species (ZM-Cd = 0.241 ± 0.011 , ZM-control = 0.242 ± 0.009 ; QM-Cd = 0.225 ± 0.009 ; QM-Control = 0.227 ± 0.007).

2.4. Two-Dimensional Gel Electrophoresis and Mass Spectrometry Identification

Protein extraction was performed as described by Péden et al. [15]. Briefly, gills ($n = 12$) were homogenised with a lysis buffer containing 7 M urea, 2M thiourea, 2% CHAPS, 32 mM dithioerythritol, 0.02% pharmalyte 3–10 NL, antiproteases (Pierce™ Protease Inhibitor), 50 mM TRIS, pH 6.8. and, for IEF (isoelectrofocusing), a total of 600 μg of proteins per sample were loaded on non-linear wide-range immobilised pH gradient strips (IPG strip pH 3–10, NL/18 cm, GE Healthcare). After IEF and equilibration steps, SDS-PAGE electrophoresis were conducted with two Protean plus Dodeca-Cell (Bio-Rad, Hercules, CA, USA) allowing a parallel run of 24 large gels (12% polyacrylamide, 20 cm \times 20 cm \times 1.5 cm).

After colloidal blue staining and scanning, gels exhibiting migration impairment were excluded and gel images were analysed using Delta 2D (Decodon, GmbH). For each spot, normality and homoscedasticity were checked (Shapiro test and F-test). Normality was always observed, but not homoscedasticity. Consequently, normalised volumes were compared between the control group and the group of mussels exposed to cadmium for each spot and each species, using either a Student *t*-test or a Welch *t*-test. Spots with a *p*-value below 0.05 were considered as differentially abundant expressed and selected for further analysis using mass spectrometry. No risk correction was applied to the computed *p*-values since spots are considered independent from each other.

2.5. Mass Spectrometry and Protein Identification

Mass spectrometry and protein identification were performed on spots of interest after trypsin digestion (Promega, Charbonnières-les-Bains, France) as described [15]. Peptides were analysed with a nano-LC1200 system coupled to a 6545XT AdvanceBio Q-TOF mass spectrometer (Agilent Technologies, Santa Clara, CA, USA). Briefly, peptides were enriched and desalted on a 160 nL C18 reversed-phase trap column and separated on a Zorbax C18 column (75 μm inner diameter \times 150 mm long, 5 μm particle size and 30 nm pore size; Agilent Technologies). MS/MS peak lists were extracted and analysed with the Xtandem pipeline (<http://pappso.inra.fr/bioinfo/xtandempipeline/>, accessed on 10 August 2023) using transcriptomic data from *Dreissena polymorpha* and *Dreissena rostriformis bugensis* [16]. Proteins were further identified by searching in the non-redundant protein sequence database with the Blastp (Basic Local Alignment Search Tool) of NCBI (<https://blast.ncbi.nlm.nih.gov/Blast.cgi/>, accessed on 10 August 2023).

2.6. Functional Protein Analysis

Functional study of proteins was performed according to UniProt (<https://www.uniprot.org/>, accessed on 10 August 2023), GeneCards (<https://www.genecards.org/>, accessed on 10 August 2023), GeneOntology (<https://amigo.geneontology.org/>, accessed on 10 August 2023), and KEGG (Kyoto Encyclopedia of Genes and Genomes) (<https://www.genome.jp/kegg/>, accessed on 10 August 2023) database analyses. Association network analysis of proteins was conducted using STRING (Search Tool for the Retrieval of Interacting Gens/Proteins, <https://string-db.org>, accessed on 6 September 2023 [17]).

For more details, the interaction map was generated from the web-based search STRING v11.0 database using default settings.

3. Results

3.1. General Overview

In order to better understand the responses and sensitivities of *Dreissena polymorpha* (ZM) and *Dreissena rostriformis bugensis* (QM) as sentinel organisms, exposure to cadmium was performed under laboratory conditions and the gill proteomes were analysed using two-dimensional electrophoresis separation (Figures S2 and S3). The differentially abundant proteoforms (DAPs) were selected for mass spectrometry analysis, with identifications based on species-specific transcriptomic data. The study investigated the effects of a 7-day exposure to cadmium at an initial concentration of $100 \mu\text{g}\cdot\text{L}^{-1}$ on the two species while maintaining a control group. Metal bioaccumulation was measured in both species at the end of the experiment. Significantly different concentrations were observed between the two species, with QM showing $37.2 \pm 9.6 \mu\text{g}\cdot\text{g}^{-1}$ dry weight and ZM showing $14.9 \pm 3.8 \mu\text{g}\cdot\text{g}^{-1}$ dry weight. This outcome is in line with a prior study that reported a higher uptake rate in QM than in ZM [18]. Principal component analysis (PCA) performed on the proteomic dataset clearly discriminated cadmium-exposed and control mussels in both species (Figure 1).

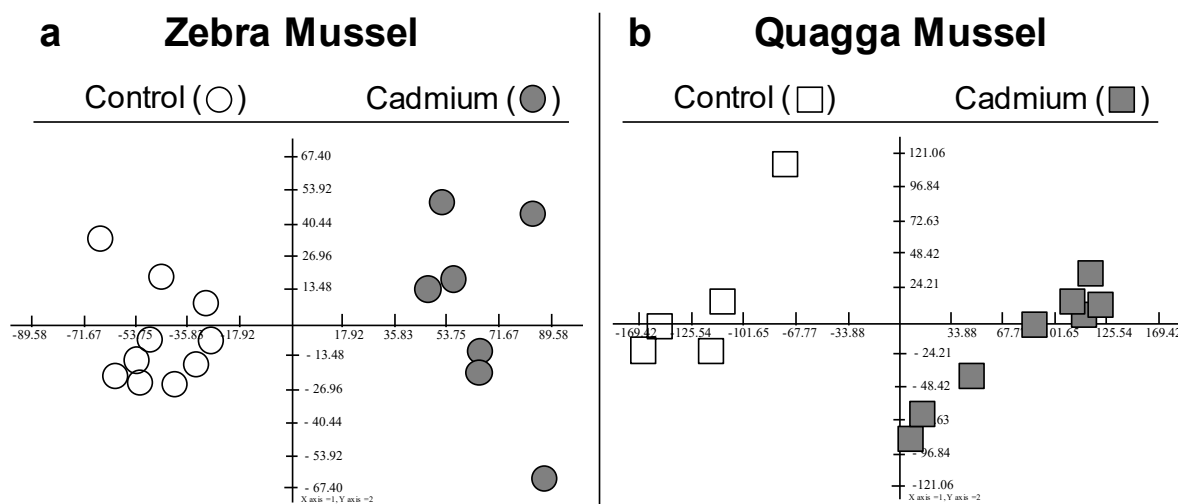


Figure 1. F1F2 Factorial planes of Principal Component Analysis (PCA) computed on normalised spot volume. (a): PCA on the 88 spots \times 17 gels obtained for ZM. F1 = 34.5%, F2 = 10%. (b): PCA on the 134 spots \times 13 gels obtained for QM. F1 = 49.2%, F2 = 9%.

For the detailed results of the ZM gill proteomics, the gel images were merged into a master gel displaying 1561 proteoforms. Of these, 88 exhibited a significant difference in protein abundance between exposed and control animals. In total, 60 were up-regulated and 28 were down-regulated (Figure 2a). Mass spectrometry allowed for the identification of 81 DAPs (Table S1). For QM, 134 of the 1419 proteoforms detected exhibited a significant difference in protein abundance between exposed and control animals, with 71 up-regulated and 63 down-regulated (Figure 2b). In total, 105 DAPs were identified by mass spectrometry (Table S2).

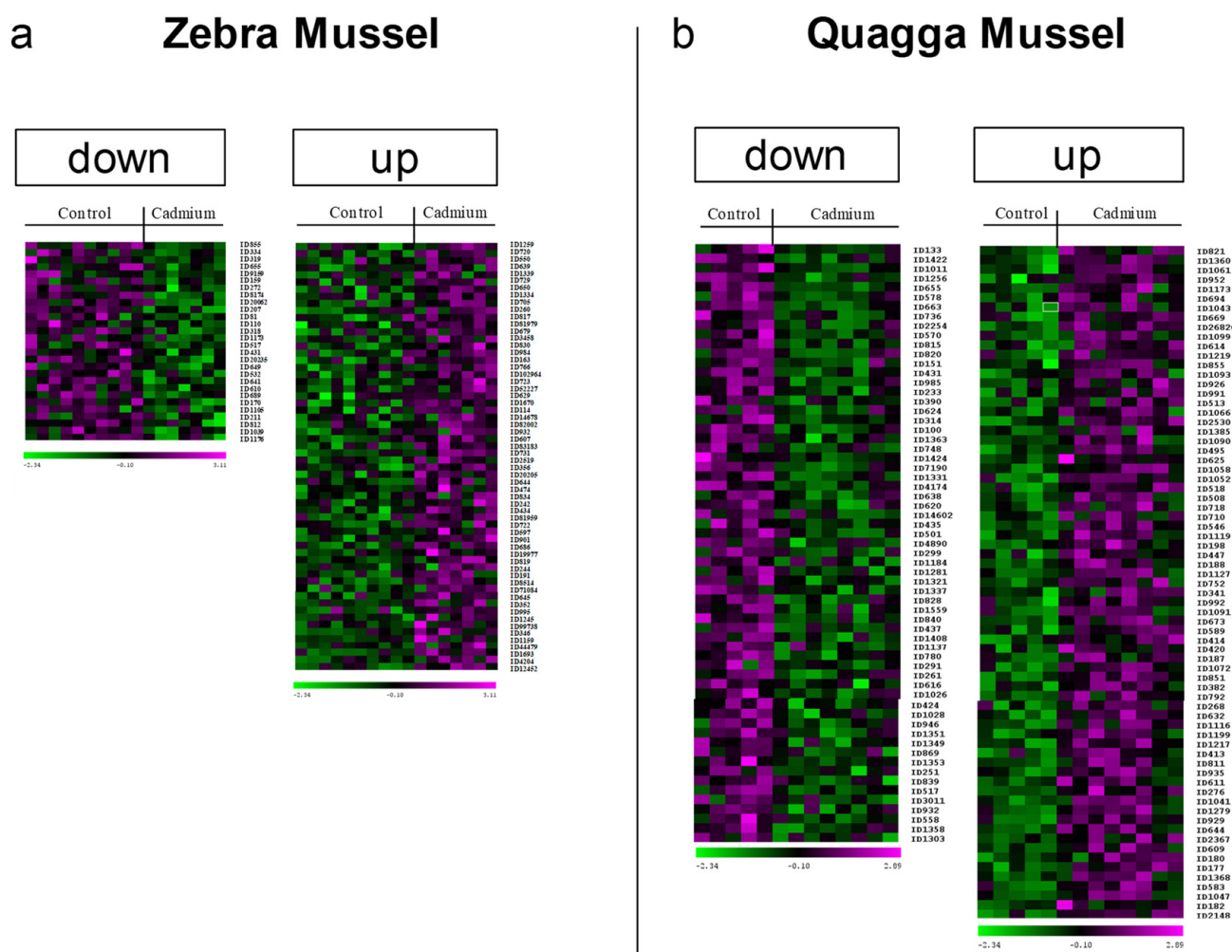


Figure 2. Heat maps of the differentially abundant gill proteoforms after cadmium exposure for (a) zebra and (b) quagga mussel. After a 7-day exposure to cadmium ($100 \mu\text{g}\cdot\text{L}^{-1}$), gill proteins from exposed and control mussels were extracted and separated by 2DE. Images were analysed using Delta 2D (Decodon, GmbH). The heat maps show the 60 up-regulated and 28 down-regulated spots in zebra mussels, and the 71 up- and 63 down-regulated spots in quagga mussels.

3.2. DAPs Classification and GO Term Enrichment Analysis

Relationships between DAPs were further investigated by using protein databases, including STRING database version 11.0 (<https://string-db.org/>, accessed on 6 September 2023), GeneCards (<https://www.genecards.org/>, accessed on 10 August 2023), UniProtKB/Swiss-Prot (<https://www.uniprot.org/>, accessed on 10 August 2023), GeneOntology (<https://amigo.geneontology.org/>, accessed on 10 August 2023) and KEGG (Kyoto Encyclopedia of Genes and Genomes) (<https://www.genome.jp/kegg/>, accessed on 10 August 2023). Determining a sole protein classification can be challenging due to their involvement in multiple cellular metabolic processes. Additionally, many proteins are multitasking or of limited knowledge. Based on our data, we classified the DAPs into five functional categories: chaperone, processing, folding, and degradation (Table 1A); calcium and cytoskeleton alterations (Table 1B); redox and detoxification (Table 1C); energy and metabolism (Table 1D); transcription and translation (Table 1E).

Table 1. Differentially abundant proteoforms identified in zebra (ZM) and quagga (QM) mussel gills after cadmium exposure.

Part A. Chaperone/processing/folding/degradation (GO:0033554 Cellular response to stress in bold)								
Sp.	label	abbrev.	Mr	pI	Var.	Identification	G.	Ca
ZM	44,479	COL12A1	83,379	5.6	2.07	collagen alpha-1(XII) chain		
ZM	346	HSPA12A	69,540	6.6	1.83	heat shock 70 kDa protein 12A		
ZM	645	PDIA6	44,461	5.6	1.68	protein disulfide-isomerase A6	1	
ZM	8514	NAPA	24,787	5.0	1.64	alpha-soluble NSF attachment protein	7	
ZM	901	TGFBI	34,177	7.4	1.52	transforming growth factor-beta-induced protein ig-h3		
ZM	434	PPP5C	56,199	6.0	1.49	serine/threonine-protein phosphatase 5	1	
ZM	2519	HSPD1	54,076	5.4	1.46	heat shock protein 60, mitochondrial	1; 6	
ZM	102,964	UFC1	23,929	6.8	1.39	ubiquitin-fold modifier-conjugating enzyme 1	1	
ZM	163	RRBP1	89,856	5.6	1.35	ribosome-binding protein 1		
ZM	984	CA2	29,793	6.1	1.34	carbonic anhydrase II	1	
ZM	817	HSPB1	38,223	6.5	1.28	small heat shock protein p36	6	
ZM	705	DNAJB11	42,109	5.7	1.26	dnaJ homolog subfamily B member 11	1	
ZM	211	HSP90AA1	85,659	5.1	0.78	heat shock protein 90	1; 6; 7	
ZM	170	MVP	89,818	5.7	0.74	major vault protein	7	
ZM	207	VCP	85,723	5.0	0.65	transitional endoplasmic reticulum ATPase	1; 6; 7	
ZM	159	HSP90B1	89,954	5.1	0.61	endoplasmic reticulum chaperone BiP GRP78	1; 6	
ZM	655	P4HB	44,315	4.4	0.56	protein disulfide-isomerase	1; 6	
ZM	334	STIP1	73,026	5.8	0.55	stress-induced-phosphoprotein 1		
QM	583	CCT5	45,634	6.1	3.34	T-complex protein 1 subunit epsilon	4	
QM	382	HSPA1	58,954	5.4	1.81	heat shock protein 70, partial	1; 4; 6; 7	
QM	851	PSMD14	34,207	6.1	1.81	26S proteasome non-ATPase regulatory subunit 14	1; 7	
QM	673	PSMC6	41,340	6.2	1.71	26S proteasome regulatory subunit 10B	1	
QM	341	ATP6V1A	63,911	5.4	1.69	V-type proton ATPase catalytic subunit A		
QM	546	HSPD1	46,798	5.5	1.61	heat shock protein 60, mitochondrial	1; 6	
QM	1058	PSMA4	28,393	5.5	1.56	proteasome subunit alpha type-4	1	
QM	625	CASP3	43,567	4.8	1.55	caspase 3 like	1; 6	
QM	1066	YWHAB	28,086	4.9	1.47	14-3-3 protein 1		
QM	839	PEPD	34,135	5.7	0.74	proline iminopeptidase	3	
QM	424	CCT4	57,096	6.2	0.70	T-complex protein 1 subunit delta	4	
QM	1026	CTSL	28,816	4.6	0.69	cathepsin L		
QM	291	HSPA1	68,940	5.4	0.67	heat shock protein 70	1; 4; 6; 7	
QM	1137	PSMA2	27,167	5.5	0.66	proteasome subunit alpha type-2	1; 7	
QM	437	ATP6V1B1	55,137	5.7	0.65	V-type proton ATPase subunit B	3	
QM	299	HSPA5	66,677	5.2	0.62	Endoplasmic reticulum chaperone BiP GRP78	1	
QM	620	CTSD	43,053	4.6	0.61	cathepsin D	6; 7	
QM	4174	PACRG	27,552	7.0	0.59	parkin coregulated gene protein homolog	1	
QM	748	P4HB	38,485	4.7	0.58	protein disulfide-isomerase	1; 6	
QM	100	MVP	94,623	5.7	0.56	major vault protein	7	
QM	985	YWHAE	29,752	4.7	0.53	14-3-3 protein epsilon	1	
QM	151	MVP	88,509	5.7	0.52	major vault protein, partial	7	
Part B. Calcium and cytoskeleton alterations (GO:0005856 Cytoskeleton in bold)								
Sp.	label	abbrev.	Mr	pI	Var.	Identification	G.	Ca
ZM	191	FLNA	85,827	6.0	1.63	filamin-A, partial	4; 6; 7	
ZM	834	PPP1CA	38,250	5.8	1.63	serine/threonine-protein phosphatase alpha-2 isoform	1; 4; 6	
ZM	244	ANXA7	78,074	7.6	1.62	annexin A7	7	Ca

Table 1. Cont.

ZM	597	PRKAR2B	45,791	4.7	1.51	cAMP-dependent protein kinase type II regulatory subunit	3; 4	
ZM	722	NME7	41,220	6.3	1.50	nucleoside diphosphate kinase 7	4	
ZM	83,183	IFI44	47,224	6.6	1.45	microtubule-associated protein 44		
ZM	932	ANXA11	33,143	5.8	1.43	annexin A11	4; 7	Ca
ZM	82,002	WDR1	64,919	6.6	1.43	WD repeat-containing protein 1	4; 7	Ca
ZM	723	TWF1	41,814	5.8	1.40	twinfilin-1	4	
ZM	766	SPAG6	40,347	5.9	1.39	sperm-associated antigen 6	4	
ZM	679	DNPEP	42,701	6.3	1.29	aspartyl aminopeptidase	7	
ZM	1334	CFL1	13,142	4.6	1.25	cofilin	4; 6	
ZM	550	SNX6	47,482	5.7	1.22	sorting nexin-6	6	
ZM	1039	TUBB	28,478	5.3	0.80	tubulin beta, partial	4; 7	
ZM	610	VAT1	45,137	5.7	0.73	synaptic vesicle membrane protein VAT-1 homolog	7	Ca
ZM	20,235	TUBA1A	46,039	5.8	0.68	tubulin alpha-1A chain	4; 7	
ZM	1173	CAPS	25,562	5.4	0.68	calcyphosin protein		Ca
ZM	110	FLNA	94,619	5.7	0.65	filamin A_B_C partial	4; 6; 7	
ZM	9159	CNN3	22,873	5.1	0.56	calponin homolog, protein unc-87	4	Ca
ZM	319	LMNA	75,067	5.2	0.55	60 kDa neurofilament protein-like	1; 4; 5; 6; 7	Ca
QM	182	CFAP58	83,075	6.6	3.75	cilia- and flagella-associated protein 58		
QM	177	PEFLIN	83,987	6.9	2.82	peflin		Ca
QM	1116	EFHD2	27,319	5.5	1.89	EF-hand domain-containing protein D2		Ca
QM	632	CROCC	43,108	6.1	1.87	rootletin	4	
QM	992	CNN3	29,595	5.3	1.70	calponin homolog, protein unc-87	4	Ca
QM	188	FLNA	83,094	5.9	1.65	filamin-A, partial	4; 6; 7	
QM	198	VCL	80,926	5.6	1.64	vinculin	4; 7	
QM	1119	CALM3	27,412	5.2	1.62	calmodulin protein 3		Ca
QM	718	CALR	39,142	4.8	1.60	calreticulin	1; 4; 5; 6	Ca
QM	508	TUBB4B	48,029	5.4	1.59	tubulin beta-4B chain	4	
QM	495	SYNE2	49,936	5.6	1.53	nesprin-2	4	
QM	1090	EFHC1	27,602	5.2	1.52	EF-hand calcium-binding domain-containing protein 1	4	Ca
QM	926	TBCB	31,668	4.8	1.42	tubulin-folding cofactor B	4	
QM	1219	TMSB10	27,111	5.3	1.39	thymosin beta	4	
QM	26,826	TUBB	27,900	4.7	1.37	tubulin beta, partial	4; 7	
QM	1360	ACTB	14,615	5.0	1.21	actin, cytoplasmic, partial	4; 6	
QM	821	TPM1	34,308	4.6	1.18	tropomyosin-1	1; 4	Ca
QM	869	CFAP161	33,433	6.0	0.73	cilia- and flagella-associated protein 161	4	
QM	1349	CALM1	17,827	4.1	0.73	calmodulin	4; 7	Ca
QM	946	TPM4	30,326	4.7	0.70	tropomyosin-4	4	Ca
QM	435	LMNA	55,491	5.3	0.61	60 kDa neurofilament protein-like	1; 4; 5; 6; 7	Ca
QM	14,602	NUDC	44,488	5.1	0.61	nuclear migration protein nudC	4	
QM	638	ACTG1	41,797	5.2	0.60	actin beta/gamma 1	4	
QM	1331	TUBB	19,149	4.7	0.58	tubulin beta, first part	4; 7	
QM	624	ACTG1	42,449	4.6	0.56	actin beta/gamma 1	4	
QM	431	LMNA	55,663	5.3	0.52	60 kDa neurofilament protein-like	1; 4; 5; 6; 7	Ca
QM	820	ANXA13	34,910	4.7	0.51	annexin A13		Ca
QM	570	ILK	46,517	6.4	0.51	integrin-linked protein kinase	4	

Table 1. Cont.

QM	815	TUBB	34,832	5.1	0.51	tubulin beta, partial	4; 7	
QM	2254	CCDC151	56,609	5.7	0.49	coiled-coil domain-containing protein 151	4	
QM	663	TUBA1A	41,535	5.7	0.48	tubulin alpha-1A chain	4	
QM	1256	DPYSL2	27,335	6.3	0.44	dihydropyrimidinase-like, partial	4	
QM	1011	ACTB	29,008	5.4	0.42	actin, cytoplasmic, partial	4; 6	
QM	133	CLCA4	93,882	5.8	0.36	calcium-activated chloride channel regulator 4A		Ca
Part C. Redox and detoxification (GO:0006790_ Sulphur compound metabolic process in bold)								
Sp.	label	abbrev.	Mr	pI	Var.	Identification	G.	Ca
ZM	4237	TALDO1	38,290	4.8	2.61	transaldolase		
ZM	4204	GLRX3	39,207	4.8	2.47	glutaredoxin-3	2	
ZM	686	CTH	42,496	6.0	1.54	cystathionine gamma-lyase	1; 2; 3; 6	Ca
ZM	81,959	PAPSS1	67,505	6.6	1.50	bifunctional 3'-phosphoadenosine 5'-phosphosulfate synthase	2	
ZM	644	ALDH1A2	44,166	5.7	1.47	retinal dehydrogenase 2	3; 6	
ZM	830	SULT1A1	37,942	5.5	1.32	sulfotransferase family 1A member 1	2	
ZM	81,979	PAPSS1	65,696	6.7	1.28	bifunctional 3'-phosphoadenosine 5'-phosphosulfate synthase	2	
ZM	650	ADH5	44,380	4.67	1.25	NADP-dependent alcohol dehydrogenase C	3	
ZM	639	BPNT1	44,175	5.8	1.23	3'(2'),5'-bisphosphate nucleotidase 1	2	
ZM	1176	SOD2	24,887	8.5	0.86	superoxide dismutase [Mn], mitochondrial	1; 2; 6	
ZM	1105	GSTZ1	26,883	5.7	0.75	maleylacetoacetate isomerase	2; 3	
ZM	517	CNDP2	48,800	5.5	0.68	cytosolic non-specific dipeptidase		
QM	1127	CNDP2	27,369	4.7	1.66	cytosolic non-specific dipeptidase		
QM	518	ALDH1A2	48,664	6.1	1.59	retinal dehydrogenase 2	3; 6	
QM	2530	SULT1A1	33,864	5.9	1.48	sulfotransferase family 1A member 1	2	
QM	1099	GST	27,684	5.9	1.38	glutathione S-transferase-like	1; 2; 3	
QM	669	CTH	41,119	6.1	1.37	cystathionine gamma-lyase	1; 2; 3; 6	Ca
QM	694	CTH	40,865	6.2	1.35	cystathionine gamma-lyase	1; 2; 3; 6	Ca
QM	1061	GSTZ1	27,873	5.4	1.23	maleylacetoacetate isomerase	1; 2; 3	
QM	1303	SOD1	21,470	5.9	0.87	superoxide dismutase [Cu/Zn]	1; 2; 4; 6; 7	
QM	558	GSS	45,618	5.8	0.77	glutathione synthetase	2; 3	
QM	1353	CYB5A	18,002	4.7	0.73	cytochrome b5	3	
QM	1351	NENF	17,075	4.7	0.71	neudesin		
QM	1028	PRDX2	28,889	6.3	0.70	peroxiredoxin-like	1; 6	
QM	840	GSR	34,032	5.9	0.65	glutathionyl-hydroquinone reductase YqjG	1; 2	
QM	1321	AHCY	20,643	6.3	0.64	adenosylhomocysteinase B	2; 3	
QM	1184	PRXL2C	27,023	5.7	0.63	dye-decolourizing peroxidase YfeX	1	
QM	736	GSTP1	38,905	5.8	0.48	glutathione S-transferase P 1	1; 2; 3; 6; 7	
QM	578	ADSS2	46,200	6.3	0.47	adenylosuccinate synthetase	3	
Part D. Energy and metabolism (GO:0019752_ Carboxylic acid metabolic process in bold)								
Sp.	label	abbrev.	Mr	pI	Var.	Identification	G.	Ca
ZM	12,452	NTPCR	26,212	5.7	2.46	cancer-related nucleoside-triphosphatase		
ZM	1159	GPD2	26,110	6.6	2.01	glycerol-3-phosphate dehydrogenase, mitochondrial		Ca
ZM	71,084	ATIC	66,279	5.9	1.65	bifunctional purine biosynthesis protein PURH	3	
ZM	242	PCCA	76,341	6.7	1.49	propionyl-CoA carboxylase alpha chain, mitochondrial	3	
ZM	20,205	FAH	44,598	5.6	1.46	fumarylacetoacetase	3	
ZM	731	PCK1_2	41,321	5.9	1.46	phosphoenolpyruvate carboxykinase [GTP], partial	1; 3	
ZM	607	FH	45,269	6.0	1.45	fumarate hydratase, mitochondrial	1; 3	
ZM	14,678	ALDOB	28,111	5.7	1.42	fructose-1, 6-bisphosphate aldolase	3	

Table 1. Cont.

ZM	114	ALDH1L1	92,374	6.0	1.41	cytosolic 10-formyltetrahydrofolate dehydrogenase	3	
ZM	1670	SPATA18	70,773	5.5	1.41	mitochondria-eating protein	1	
ZM	1339	ATP5F1D	12,048	4.4	1.23	ATP synthase delta chain, mitochondrial		
ZM	729	HPD	41,675	5.7	1.23	4-hydroxyphenylpyruvate dioxygenase	3	
ZM	720	MYG1	41,996	5.5	1.21	UPF0160 protein MYG1, mitochondrial		
ZM	812	HIBCH	38,744	6.2	0.78	3-hydroxyisobutyryl-CoA hydrolase, mitochondrial	3	
ZM	641	CKB	43,718	7.0	0.71	arginine kinase	3	
ZM	532	PCYT2	47,622	6.3	0.70	ethanolamine-phosphate cytidyltransferase		
ZM	318	PCK1	71,984	6.7	0.66	phosphoenolpyruvate carboxykinase, cytosolic [GTP]	1; 3	
ZM	20,062	LDHB	42,852	5.6	0.64	opine/octopine dehydrogenase, tauropine dehydrogenase	3	
ZM	272	GBA2	79,092	4.6	0.62	glucosidase 2 subunit beta	3	
QM	609	TKTL2_short	44,391	6.1	2.67	transketolase protein 2, partial		
QM	2367	CS	40,656	6.4	2.47	citrate synthase, mitochondrial	3	
QM	276	PCK1	69,690	6.4	2.25	phosphoenolpyruvate carboxykinase [GTP]	1; 3	
QM	611	AK5	43,717	5.8	2.24	adenylate kinase isoenzyme 5		
QM	811	MDH1B	35,684	6.3	2.06	malate dehydrogenase, cytosolic	3	
QM	1217	MDH1B	27,069	4.7	1.96	malate dehydrogenase, cytosolic	3	
QM	792	GAPDH	35,711	6.2	1.84	glyceraldehyde-3-phosphate dehydrogenase	3; 4; 5	
QM	420	MCCC2	56,870	6.7	1.76	3-methylcrotonoyl-CoA carboxylase beta chain, mitochondrial	2; 3	
QM	752	PCK1_2	37,948	5.8	1.69	phosphoenolpyruvate carboxykinase [GTP]	1; 3	
QM	1385	NIPSNAP1	14,360	6.5	1.49	protein NipSnap	7	Ca
QM	513	SHMT1	49,003	6.5	1.47	serine hydroxymethyltransferase, cytosolic	3; 5	
QM	855	IMPA1	33,752	5.4	1.40	inositol monophosphatase		
QM	1358	COX6B1	16,778	6.0	0.78	cytochrome c oxidase subunit 6B1		
QM	932	PHB1	31,386	5.4	0.76	prohibitin	6	
QM	517	ENO1	48,104	5.8	0.76	enolase	3; 6	
QM	616	SPATA18	43,782	5.3	0.69	mitochondria-eating protein	1	
QM	1408	ATP5F1D	12,863	4.6	0.65	ATP synthase delta chain, mitochondrial		
QM	828	ENO1_short	34,988	5.5	0.64	enolase-short form alias c-myc promoter-binding protein-1	3; 6	
QM	1281	MDH2	24,327	6.4	0.64	malate dehydrogenase, mitochondrial	3	
QM	501	ATP5F1B	50,871	5.1	0.61	ATP synthase subunit beta, mitochondrial		
QM	7190	ENO1	39,080	5.5	0.58	enolase	3; 6	
QM	314	TKTL2	65,910	6.0	0.56	transketolase protein 2		
QM	655	PCCB	41,805	5.3	0.45	propionyl-CoA carboxylase beta chain, mitochondrial	2; 3	
Part E. Transcription/translation (GO:0006417_ Regulation of translation in bold)								
Sp.	label	abbrev.	Mr	pI	Var.	Identification	G.	Ca
ZM	995	EIF3F	29,818	5.4	1.71	eukaryotic translation initiation factor 3 subunit F	5	
ZM	352	DDX3X	66,641	6.1	1.69	ATP-dependent RNA helicase DDX3X	1; 5; 6; 7	
ZM	819	EEF2_short	38,350	5.9	1.58	elongation factor 2, partial	1; 5; 7	
ZM	19,977	FAM172A	44,808	5.8	1.54	cotranscriptional regulator FAM172A		
ZM	474	U2AF2	53,138	5.6	1.48	splicing factor U2AF 50 kDa subunit		
ZM	356	FARSB	69,076	5.4	1.46	phenylalanine-tRNA ligase beta subunit	3	
ZM	629	PA2G4	44,025	6.3	1.41	proliferation-associated protein 2G4	5; 6; 7	
ZM	260	FUBP1	76,901	6.0	1.27	far upstream element-binding protein 1		
ZM	1259	EIF5A	20,524	5.0	1.18	eukaryotic translation initiation factor 5A	5; 6	
ZM	649	WARS1	43,779	5.96	0.70	tryptophanyl-tRNA synthetase, cytoplasmic	3	
ZM	431	NAPIL1	60,086	4.3	0.68	nucleosome assembly protein 1 1		

Table 1. Cont.

ZM	81	EEF2	93,962	7.5	0.65	elongation factor 2	1; 5
QM	644	WARS1	42,768	5.8	2.44	tryptophanyl-tRNA synthetase, cytoplasmic	3
QM	710	EIF4A1	39,889	5.8	1.60	eukaryotic initiation factor 4A-I	5
QM	991	EIF4B	29,725	5.6	1.44	eukaryotic translation initiation factor 4B	5
QM	614	PA2G4	43,956	6.3	1.39	proliferation-associated protein 2G4	3; 5; 7
QM	952	EIF3F	30,865	5.5	1.28	eukaryotic translation initiation factor 3 subunit F	5
QM	261	FUBP1	70,697	5.7	0.68	far upstream element-binding protein 1	
QM	780	DDX3X	37,130	6.3	0.66	ATP-dependent RNA helicase DDX3X	1; 5; 6; 7
QM	1559	ELOB	21,107	4.6	0.65	elongin B	1
QM	1422	RIDA	11,327	6.0	0.40	2-iminobutanoate/2-iminopropanoate deaminase	3; 5

Legend: Sp., ZM for zebra mussel, QM for quagga mussel; labels correspond to the reference number of the DAP in the proteomic analysis; abbrev. refer to GeneCards abbreviation by similarity; Mr and pI are observed DAP molecular mass and isoelectric point, respectively; var. greater than 1 indicates an increase in abundance of proteoforms after cadmium exposure, and conversely, a decrease for values lower than 1. Table 1 presents the five functional categories: chaperone, processing, folding, and degradation (A); calcium and cytoskeleton alterations (B); redox and detoxification (C); energy and metabolism (D); transcription and translation (E). G. columns refer to Gene Ontology terms: G1. GO:0033554_Cellular response to stress; G2. GO:0006790_Sulfur compound metabolic process; G3. GO:0019752_Carboxylic acid metabolic process; G4. GO:0005856_Cytoskeleton and G5. GO:0006417_Regulation of translation; G6. GO:0042981_Regulation of apoptotic process; G7. GO:0045055_Regulated exocytosis; Ca for calcium dependant protein. A colour version including observed MW and pI is proposed in Table S3.

Additionally, a GO term enrichment analysis was performed, allowing the association of biological processes with each DAP (Table S4, Figures S4 and S5). The analysis results highlighted seven major biological processes, as follows: G1.GO:0033554_Cellular response to stress (21 DAPs for ZM, 30 DAPs for QM), G2.GO:0006790_Sulfur compound metabolic process (7 DAPs for ZM, 12 DAPs for QM), G3.GO:0019752_Carboxylic acid metabolic process (20 DAPs for ZM, 27 DAPs for QM), G4.GO:0005856_Cytoskeleton (14 DAPs for ZM, 35 DAPs for QM), G5.GO:0006417_Regulation of translation (7 DAPs for ZM, 11 DAPs for QM), G6.GO:0042981_Regulation of apoptotic process (18 DAPs for ZM, 23 DAPs for QM) and G7.GO:0045055_Regulated exocytosis (17 DAP for ZM, 20 DAPs for QM) (Figure 3).

Cadmium is known to interfere with calcium signalling pathway. Thus, we searched for calcium-dependent proteins in the DAPs. At least 17 DAPs were found to be calcium-dependent, corresponding to 14 proteins (ANXA7, ANXA11, ANXA13, CAMK1, CALM1, CALR, CAPSL, CLCA4, CNN3, EFHC1, EFHD2, PEFLIN, TPM1, TPM4, WDR1, and VAT1) (Table 1). Regarding ZM, ANXA7, ANXA11, and WDR1 displayed increases in abundance, whereas VAT1, CAPSL, and CNN3 were decreased. Concerning QM, CNN3, EFHC1, EFHD2, PEFLIN, CAMK1, CALR, NIPSNAP1, and TPM1 increased in abundance whilst CALM1, TPM4 CLCA4, and ANXA13 showed a decrease (Table 1, last column).

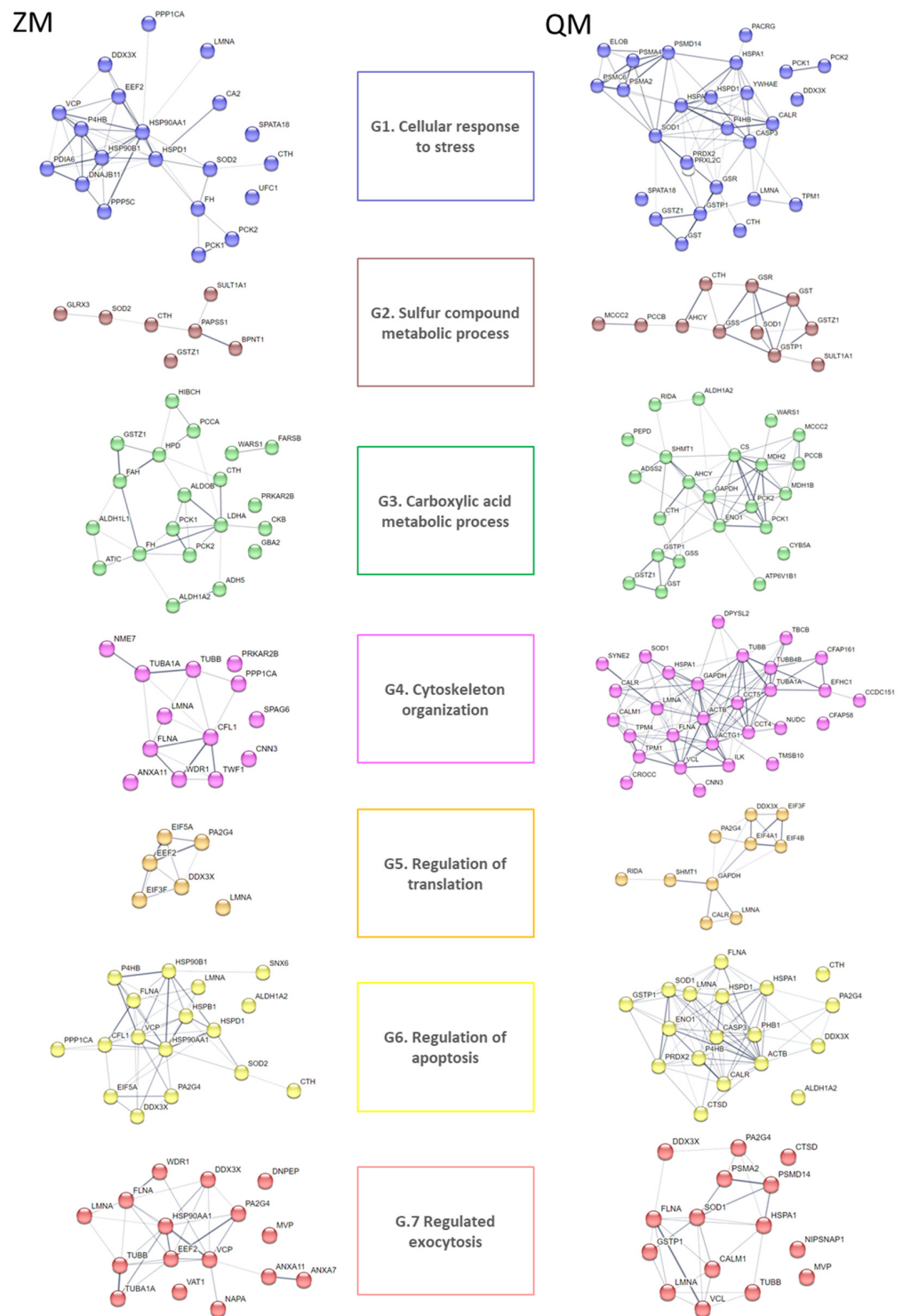


Figure 3. STRING analysis of cadmium-induced DAPs for zebra (ZM) and quagga (QM) mussels. Protein–protein interaction networks were constructed using the STRING database (<https://string-db.org>, accessed on 6 September 2023) [17]). Nodes in the network represent DAPs. Protein abbreviations are reported in Table 1. Confidence in protein interactions is shown by the thickness of the lines connecting each node. G refers to Gene Ontology terms: G1. GO:0033554_Cellular response to stress; G2. GO:0006790_Sulfur compound metabolic process; G3. GO:0019752_Carboxylic acid metabolic process; G4. GO:0005856_Cytoskeleton and G5. GO:0006417_Regulation of translation; G6. GO:0042981_Regulation of apoptotic process; G7. GO:0045055_Regulated exocytosis.

3.3. Shared Protein Identity between the Two Species

Over and above the differences, identical proteins were found in ZM and QM. Their abundance after exposure to cadmium varied either in the same direction (12 proteins) or in opposite directions (10 proteins, Table 2).

Table 2. DAPs sharing similar protein identities.

Variations	Abbreviation	Protein	
Abundances change in the same direction	Up	ALDH1A2	retinal dehydrogenase 2
		CTH	cystathionine gamma-lyase
		EIF3F	eukaryotic translation initiation factor 3 subunit F
		FLNA	filamin-A, partial
		HSPD1	heat shock protein 60, mitochondrial
		PA2G4	proliferation-associated protein 2G4
	Down	PCK1	phosphoenolpyruvate carboxykinase [GTP], partial
		SULT1A1	sulfotransferase family 1A member 1
		LMNA	60 kDa neurofilament protein-like
		MVP	major vault protein
		P4HB	protein disulfide-isomerase
		TUBA	tubulin alpha subunit
Abundances change in opposite directions	ZM Up QM Down	ATP5F1D	ATP synthase delta chain, mitochondrial
		DDX3X	ATP-dependent RNA helicase DDX3X
		FUBP1	far upstream element-binding protein 1
		SPATA18	mitochondria-eating protein
	ZM Down QM Up	CNDP2	cytosolic non-specific dipeptidase
		CNN3	calponin homolog, protein unc-87
		GSTZ1	maleylacetoacetate isomerase alias GST Z
		WARS1	tryptophanyl-tRNA synthetase, cytoplasmic
		PCK1	phosphoenolpyruvate carboxykinase, cytosolic [GTP]
		TUBB	tubulin beta, partial

Among the proteins with similar variations, increases in abundance were the most numerous, namely retinal dehydrogenase 2, cystathionine gamma lyase, eukaryotic translation initiation factor 3 subunit F, filamin A, heat shock protein 60, proliferation-associated protein 2G4, sulfotransferase family cytosolic 1A member 1, and phosphoenolpyruvate carboxykinase, partial. On the other hand, common decreases in abundance concerned 60kDa neurofilament protein, major vault protein, protein disulfite isomerase, and tubulin subunits.

The proteins showing an increase in abundance in QM and a decrease in ZM were mitochondrial ATP synthase delta chain, ATP-dependent RNA helicase DDX3X, far upstream element-binding protein 1, and mitochondria-eating protein. Finally, the proteins showing an increase in abundance in ZM and a decrease in QM were cytosolic non-specific dipeptidase, calponin homolog protein unc-87, maleylacetoacetate isomerase, cytoplasmic tryptophanyl-tRNA synthetase, cytosolic [GTP] phosphoenolpyruvate carboxykinase, and tubulin beta, partial. The proteins referred to as partial correspond to DAPs exhibiting a lower MW than expected.

3.4. Evidence of Short Proteoforms

It is noteworthy that in both species, some of the identified DAPs had a much lower molecular mass than expected, suggesting truncated proteins or alternative splicing events. It remains unclear whether the proteoforms have any other non-canonical functions [19]. Shorter proteoforms correspond mainly to cytoskeleton components such as alpha and beta

tubulin subunits or filamin. Cadmium significantly impacts cytoskeleton elements which can impair cytoskeleton organisation [20]. Examples of cytoskeleton short proteoforms are presented in Figure S6.

Other shorter proteoforms are related to the phosphoenolpyruvate kinase enzyme (PCK). DAP QM 752 and DAP ZM 731 are approximately 40 kDa PCK proteoforms, while the standard PCK weighs around 70 kDa. Two DAPs corresponding to the full-length protein have also been identified, namely DAP QM 276 and DAP ZM 318. The presence of the shorter forms was confirmed through at least two gel excisions. MS data analysis using the Xtandem! pipeline showed that the shorter forms correspond to the second part of the enzyme in both species. It also confirmed a full sequence coverage for the 70 kDa proteoforms (Figure 4). The missing part in short proteoforms includes the active site, suggesting loss of enzyme activity after a proteolytic cleavage. The two truncated forms of PCK start at the metal binding site of the protein, but their formation cannot be explained, except that the PCK cofactor is the divalent ion manganese. It is possible for cadmium to replace manganese or disrupt its function. At least 2 PCK isoforms have been described, one cytosolic (PCK1) and the other mitochondrial (PCK2). They differ mainly in the first part of their sequence, so we could not establish whether the 40 kDa proteoforms originate from a cytosolic or mitochondrial PCK.

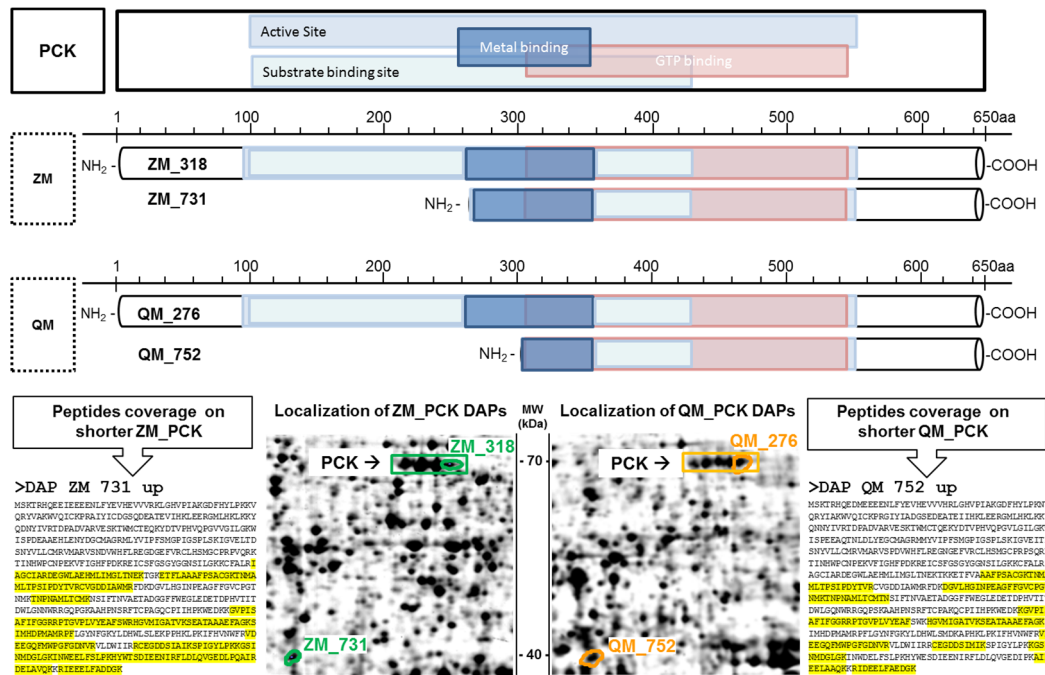


Figure 4. Shorter phosphoenolpyruvate kinase enzyme (PCK) proteoforms are more abundant after cadmium exposure. Structure of full-length PCK and shorter proteoforms of quagga (QM) and zebra (ZM) mussels. Top: PCK functional domains (NCBI CD batch search). Bottom: DAP localisation on 2DE gels; sequence coverage is highlighted in yellow.

A third type of a short proteoform corresponding to XP_052223977.1 and named 60 kDa neurofilament protein-like (alias LMNA, lamin-A) was observed. Both species exhibited a decrease in abundance for the DAPs which were identified as 60 kDa neurofilament protein-like. However, these DAPs did not exhibit the same molecular weight (approximately 70 kDa for DAP ZM 319 and 55 kDa for DAPs QM 431 and 435). In QM gels, we also identified a spot (QM 250) which remains constant and corresponds to the 70 kDa form of the 60 kDa neurofilament protein-like (Figure 5). In fact, XP_052223977.1 is a 70 kDa lamin precursor of intermediate filament. Its cleavage leads to lamin A/C, a component of the nuclear lamina. Alternative splicing events may explain the existence of DAPs with molecular weights less than 70 kDa.

Spot QM 250

71 kDa / pI 5.26 - no DAP

> QM contig XP_052223977.1 homolog

MASESTDFSTRKRQSMGPGSVIVQKTA PGLRMSLGGGQGMTTT
 IRRNVVQSNYAAPNRPVGEAGKVSKE SVATV LNTRGHEKKELG
 DLNSKLANYIDKVKYMEACNKAMTEEIDRLRKMKGYTQDRIKE
 EYEEELKEARATINTLSKEIAPLQARI LKLDKVDVSDQEQEINM
 LKHKHDDLQGGVQKLNQLIGDLEGE L ATLRNQLDAMGKENDML
 KQDNLRLRDDNER IREDFEAAVTQINAENERDALAEELQFTQ
 DTLNAEIEELRSLTNFKSVQPD IQMVKSEFKDCIQAIQAEY
 NDQLSKMTDSTERRCQERIASMENAFRRDNTDSSVTKTENKTL
 KSALSDNKS KIADLQRENDRLRKELEDLQYRFDEADRQCDEDK
 DTLRMQLAALEQDLAEVMHDLEGMKSHNLDLELEIACYRKLE
 GEENSMKRIEDQAKLQSEGG AQLSQI IAGGKKGSSSQTSSS
 YSRSGGMSSSGGGGGMSSVSMSESTGMVKVSKSKCAVTF A
 EVAQDGSFVRENGSPSKDFDLSKWSISRRHPRGTSSFEFPEN
 FKLT PKQSLRI FAYSFSDEAKTGDLIADKANCNSWGTGNGEYT
 LLDDKANEKATSKLEYAAAR

Spot QM 435

55 kDa / pI 5.26 - down

> QM contig XP_052223977.1 homolog

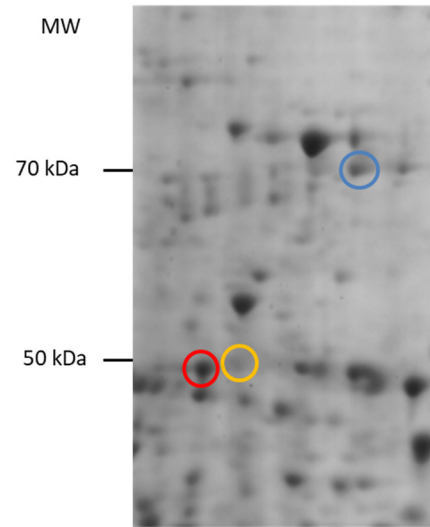
MASESTDFSTRKRQSMGPGSVIVQKTA PGLRMSLGGGQGMTTT
 IRRNVVQSNYAAPNRPVGEAGKVSKE SVATV LNTRGHEKKELG
 DLNSKLANYIDKVKYMEACNKAMTEEIDRLRKMKGYTQDRIKE
 EYEEELKEARATINTLSKEIAPLQARI LKLDKVDVSDQEQEINM
 LKHKHDDLQGGVQKLNQLIGDLEGE L ATLRNQLDAMGKENDML
 KQDNLRLRDDNER IREDFEAAVTQINAENERDALAEELQFTQ
 DTLNAEIEELRSLTNFKSVQPD IQMVKSEFKDCIQAIQAEY
 NDQLSKMTDSTERRCQERIASMENAFRRDNTDSSVTKTENKTL
 KSALSDNKS KIADLQRENDRLRKELEDLQYRFDEADRQCDEDK
 DTLRMQLAALEQDLAEVMHDLEGMKSHNLDLELEIACYRKLE
 GEENSMKRIEDQAKLQSEGG AQLSQI IAGGKKGSSSQTSSS
 YSRSGGMSSSGGGGGMSSVSMSESTGMVKVSKSKCAVTF A
 EVAQDGSFVRENGSPSKDFDLSKWSISRRHPRGTSSFEFPEN
 FKLT PKQSLRI FAYSFSDEAKTGDLIADKANCNSWGTGNGEYT
 LLDDKANEKATSKLEYAAAR

Spot QM 431

56 kDa / pI 5.30 - down

> QM contig XP_052223977.1 homolog

MASESTDFSTRKRQSMGPGSVIVQKTA PGLRMSLGGGQGMTTT
 IRRNVVQSNYAAPNRPVGEAGKVSKE SVATV LNTRGHEKKELG
 DLNSKLANYIDKVKYMEACNKAMTEEIDRLRKMKGYTQDRIKE
 EYEEELKEARATINTLSKEIAPLQARI LKLDKVDVSDQEQEINM
 LKHKHDDLQGGVQKLNQLIGDLEGE L ATLRNQLDAMGKENDML
 KQDNLRLRDDNER IREDFEAAVTQINAENERDALAEELQFTQ
 DTLNAEIEELRSLTNFKSVQPD IQMVKSEFKDCIQAIQAEY
 NDQLSKMTDSTERRCQERIASMENAFRRDNTDSSVTKTENKTL
 KSALSDNKS KIADLQRENDRLRKELEDLQYRFDEADRQCDEDK
 DTLRMQLAALEQDLAEVMHDLEGMKSHNLDLELEIACYRKLE
 GEENSMKRIEDQAKLQSEGG AQLSQI IAGGKKGSSSQTSSS
 YSRSGGMSSSGGGGGMSSVSMSESTGMVKVSKSKCAVTF A
 EVAQDGSFVRENGSPSKDFDLSKWSISRRHPRGTSSFEFPEN
 FKLT PKQSLRI FAYSFSDEAKTGDLIADKANCNSWGTGNGEYT
 LLDDKANEKATSKLEYAAAR



ZM NCBI XP_052223977.1 sequence

MTSESEFSTRKRQSMGPGSVIVQKTA PGLRMSLGGNLGSS
 MTIRRVVVTSTYAAPNRPVGEAGKVSKE SVATV MNTRGKEK
 RDLGDLNSKLANYIDKVKYMEACNKAMTEEIDRLRKMKGYT
 QDRVKEEYEEELKEARATIDTLSKEIAPLQAKI LKLEDKVD
 SQQQENMLKHKHDE LQGGVQKLNQLIGDLEGE L ATLRNQL
 DAMGRENDMLKQDNLRLREDNDR IREDFEAAVTQINAENE
 RDALAEELQFTQDTLNAEIEELRSLTNFKSVQPD IQMVK
 SEFKDCIQAIQAEYNDQLAKMTESTERRCQERI SSMENAFR
 RDNTDSSITKTENKTLKSLQGDNKGMRADLQRENDRLRKE
 EDLQNRLLDDECRQCEEDKDTLRQLQALEADLAEVMHDLE
 MKSHNLDLELEIACYRKLEGEENSMKRIEDQAKLQSEGG
 AQLAGIIAGGR.GGSSSQTSSSYSRSGGMSMGGGGGMSS
 MSSMSESTGMVKVSKSKCAVTF AEVAQDGSFVRENGSPS
 KDFDLSKWSITRRHPRGTSSFEFPDNFKLTPKQSLRI FAYS
 FSDDAKSGDLIADKASCNSWGTGNGEYTLDDKANEKATSK
 LEYAAAR

(in red, residues common between QM and ZM sequences)

SmartBlast Result:

An intermediate filament similar to lamin

<https://blast.ncbi.nlm.nih.gov/smartblast> (accessed on 10th August 2023)



Figure 5. Several proteoforms for one protein: the case of a 60 kDa neurofilament protein-like. In quagga mussel (QM), several spots were identified using homology with the zebra mussel (ZM) XP_052223977.1 sequence: Spots 250, 435 and 431. Spot 250 is a 71 kDa protein and probably the precursor form of the 60 kDa neurofilament protein (blue circle on the 2DE gel). It presented no variation after cadmium exposure. Spots 435 and 431 are shorter sequences of 55 kDa (red and orange circles on the 2DE gel, respectively), corresponding to the first part of the XP_052223977.1 sequence (see MS peptide coverage highlighted in yellow). The XP_052223977.1 sequence of the 60 kDa neurofilament protein-like of ZM is presented in the black box, with the NCBI Smartblast result showing its alignment with lamins.

A fourth type of short proteoform corresponds to an approximately 50 kDa HSP70 (Figure S7). Detected solely in QM, its abundance is increased in response to cadmium

exposure. Stable fragments of HSP70 have previously been evidenced in other studies, particularly in gills of blue mussels after acute heat stress [21]. It is unclear whether these truncated HSP70 proteoforms play a role during stressful conditions or whether they are indicative of an increasing level of intracellular proteolysis, which is more likely given the presence of other short proteoforms in QM gills exposed to cadmium.

Finally, a 37 kDa DAP QM 828 was identified as enolase (ENO1) whereas the canonical enzyme has a molecular mass of 48 kDa. MS analysis showed that this DAP lacks the first part of the ENO-1 (Figure 6a).

a. DAP QM 828 : ENO1_short

DAP QM 828 (35 kDa / pI 5.5) down

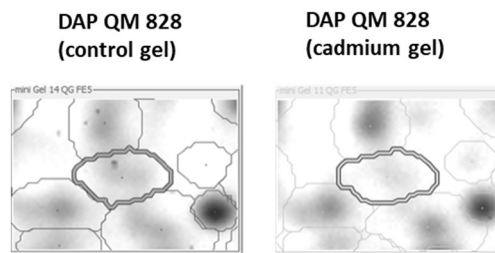
> Enolase

MPVKTVRRARQIFDSRGNPTVEVDVTEKGLFRAAVPSGASTGIYEALMRDKD
 PKAYHKGVMNANVNNVNI IAGELVKAGLDEADQTAVDEFLGLDGTENKSKL
 GANA ILGVSLAVCKAGAARKGVPLRYRHADLAGNTEVILPVPFANVINGGSHA
 GNK LAMQEFMILP IGASSFSEAMRMGSEVYHHLK DVIKKKYGDACNVGDEGG
 FAPN ILENDEGLALCKTAIEKAGYTGK IMIGMDVAASEFCCKDGLYDLDFKND
 SKKEDWLTSDK LADVYQSFIKNYPVIVSIEDPFDQDDWAAYTKLTSNVKIQIVG
 DDL LVTNPKRVQTGIDKRCNCLLLKVNQIGSVTESIKAWRMKDEGWGMVMS
 HRSGETEDTFIADLVVGLCTGQIKTGAPCRSERLAKYNQILRIEELGSKAKF
 AGTNFRYPYGGK

Coverage: 28%

Evalue: -45.481716

Theoretical pI/Mw: 5.83 / 47309.05



b. SmartBlast Result with the coverage part of the DAP QM 828

DOMAINS: and other(s) domains

Enolase

Your query: unnamed protein product DAP QM 828

c-myc promoter-binding protein-1 isoform MBP-1

enolase 1B, retrotransposed

enolase 1b, (alpha)

enolase, isoform F



c. DAP QM 517 : full lenght ENO1 sequence

DAP QM 517 (48 kDa / pI 5.8) down

> Enolase

MPVKTVRRARQIFDSRGNPTVEVDVTEKGLFRAAVPSGASTGIYEALMRDKD
 PKAYHKGVMNANVNNVNI IAGELVKAGLDEADQTAVDEFLGLDGTENKSKL
 GANA ILGVSLAVCKAGAARKGVPLRYRHADLAGNTEVILPVPFANVINGGSHA
 GNK LAMQEFMILP IGASSFSEAMRMGSEVYHHLK DVIKKKYGDACNVGDEGG
 FAPN ILENDEGLALCKTAIEKAGYTGK IMIGMDVAASEFCCKDGLYDLDFKND
 SKKEDWLTSDK LADVYQSFIKNYPVIVSIEDPFDQDDWAAYTKLTSNVKIQIVG
 DDL LVTNPKRVQTGIDKRCNCLLLKVNQIGSVTESIKAWRMKDEGWGMVMS
 HRSGETEDTFIADLVVGLCTGQIKTGAPCRSERLAKYNQILRIEELGSKAKF
 AGTNFRYPYGGK

Coverage: 81%

Evalue: -226.84058

Theoretical pI/Mw: 5.83 / 47309.05

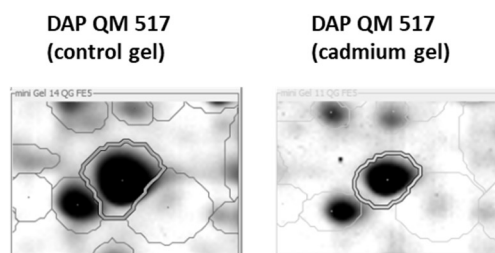


Figure 6. A quagga mussel (QM) shorter enolase proteoform is a putative c-myc promoter-binding protein-1 isoform. (a) 37 kDa DAP QM 828 was identified as enolase (ENO1) and lacks the first part of the enzyme; (b) the shorter enolase is highly similar to the c-myc promoter-binding protein-1 isoform (MBP-1); (c) 48 kDa DAP QM 517 is also identified as enolase; coverage (highlighted in yellow) on the full-length sequence confirms this DAP correspond to the whole enzyme.

Furthermore, the 37 kDa DAP QM 828 is highly similar to an alternative splicing isoform called c-myc promoter-binding protein-1 isoform (MBP-1), a tumour suppressor (Figure 6b). Using an alternative start codon, the ENO1 gene can produce a truncated 37 kDa protein, mainly localised in the nucleus. MBP-1 lacks the first 96 amino acids present in ENO1 and its primary function is to bind to the c-myc transcription factor and suppress

its activity [19]. Further experimentations are required to clarify the synthesis of the short ENO1 proteoform and its potential function. It is worth noting that after cadmium exposure, another DAP was also identified as ENO1, DAP QM 517. This proteoform was of 48 kDa, and exhibited complete coverage of the enolase sequence, indicating that the DAP QM 517 corresponds to the entire enzyme (Figure 6c). Finally, it should be highlighted that enolase, regardless of its form, was found to undergo modifications upon exposure to cadmium stress, as shown in numerous studies in both vertebrates and invertebrates [22–25].

4. Discussion

The objective of this work was to compare the responses of two sister species (*Dreissena* sp.) under stress by carrying out quantitative comparisons of the gill tissue at protein level. In theory, proteomics makes it possible to compare all the proteins in a tissue, but in practice, technical limitations reduce the number of actually compared proteins. Without being exhaustive, the extraction and separation conditions used here favour soluble proteins and offer better resolution for proteins with isoelectric points between four and seven and molecular weights between 10 and 100 kDa. In addition, the 2DE approach mainly reveals the most abundant proteins in the tissue and, as a result, modifications of proteins involved in basic cellular metabolism as well as in cellular trafficking and organisation were easily detected. However, gel-based proteomic analysis has the advantage of being an open approach capable of highlighting post-translational modifications (PTMs) which are very important in cellular homeostasis [26]. Regarding PTMs, not all of them are directly detectable on 2D gels, but only those that result in a sufficiently large change in molecular weight and/or isoelectric point to appear distinct from the main proteoform of the identified protein. It should be noted that several DAPs share the same identification, which means that first, the total number of identified proteins is much lower than the number of modified proteoforms, and second that post-transcriptional and/or post-translational modifications were involved in the response following cadmium exposure. Interestingly, the extent of the response differed between the sister species with 5.6% of varying proteoforms for ZM and 9.4% for QM, a difference mainly explained by a doubling of under-expressed proteoforms in QM. Therefore, proteomic analysis revealed a higher effect of cadmium on QM gill proteome than on ZM gill one, consistent with the higher accumulation of the metal in QM tissues at the end of the experiment.

4.1. DAP Classification and Protein Identification

The review of the literature regarding the identified proteins offers supporting information to comprehend our observations. Therefore, when interpreting the results, we considered the effect of cadmium, the identity of the protein, and the likelihood of it being a modified proteoform. Considering the scarcity of information available on bivalves in general and in mussels more specifically, we incorporated homology-based information as it pertains to humans and used GeneCards abbreviations for the database search. Then, the data were processed utilizing previously established bibliographic records on the effects of cadmium and our understanding of the bivalve physiology [20,27–32].

In some instances, there was no correspondence between the mussel protein and a human protein, which led us to assign a default GeneCards abbreviation. This was the scenario for ZM 641 DAP, which was recognised as an arginine kinase responsible for reversibly catalysing the transfer of phosphate between ATP and the phosphogen arginine phosphate in invertebrates, similar to creatine kinase (CKB) and the phosphogen creatine phosphate found in vertebrates. Arginine kinase and creatine kinase have a crucial function in the energy transduction process of tissues with high and varying energy needs, such as those in mussel gills [15,33]. It is noteworthy that this tissue is involved in osmoregulation in bivalves, where free amino acids, including taurine, aspartate, alanine, glutamate, glycine, and arginine, act as organic osmolytes [34,35]. Likewise, we assigned the abbreviation LDHB1 (lactate dehydrogenase) to DAB ZM 20062, identified as octopine dehydrogenase (EC 1.5.1.11), for which the KEGG pathway is also related to the metabolism of arginine

and proline [36]. In all cases, the interpretation of the results was based solely on the knowledge of the identified protein and not on any arbitrary correspondence. Not all of the proteins identified are discussed in the text. However, for each protein, a concise summary of information gathered from GeneCards is provided in Supplementary Materials (<https://www.genecards.org>, accessed on 10 August 2023), also including bibliographic references related to cadmium exposure (Table S5).

4.2. Proteome Responses to Cadmium Exposure

In aquatic organisms, cadmium can be absorbed via digestion or internalised by the gills, borrowing calcium or other metal transporters. At the cellular level, cadmium has pleiotropic toxic effects that alter the homeostasis of calcium and essential divalent metals, the redox state with an overproduction of reactive oxygen species leading to the oxidation of macromolecules such as proteins, lipids, and DNA along with an impairment of DNA repair mechanisms, thus activating apoptosis and cell death [27,30,31].

At the molecular level, the cadmium cation shares chemical properties with other divalent ions (e.g., Zn^{2+} , Fe^{2+} , Ca^{2+}) allowing for it to cross biological barriers and accumulate in tissues. In cells, the substitution of an essential metal ion, e.g., zinc or manganese, can occur during the folding process of nascent polypeptide chains, which may have an impact on their biological activity. Moreover, cadmium interacts with sulfhydryl groups and can lead to the alteration of proteins containing thiol groups and the depletion of reduced glutathione [37–39].

Oxidative stress is a major mechanism leading to cadmium-induced tissue damages. By competing with essential metal ions (e.g., Cu^{2+} , Fe^{2+} , Mn^{2+} , Zn^{2+}), cadmium increases cellular concentrations of free metal capable of a Fenton-type reaction and, by interacting with reduced glutathione, it decreases antioxidant defences, thereby promoting the oxidative action of reactive oxygen species [20,26–32,40,41].

The DAPs identified in both species mirror the aforementioned differential effects of the toxicant. Analysis of GO enrichment revealed strategies shared by and unique to both species in response to Cd exposure. In short, both species share the following cellular processes: induction of the cellular response to stress (GO:0033554), involvement of components of sulphur metabolism (GO:0006790), regulation of the apoptotic process (GO:0042981) and of translation (GO:0006417), changes in the generation of precursor metabolites and energy (GO:0006091), changes in the organisation of the cytoskeleton (GO:0000226, for microtubules; GO:0030036 for actin), and enhancement of exocytosis processes (GO:0045055) (Table S4; Figure 7).

Noticeably, in ZM only, GO enrichment analysis highlighted a response to inorganic substance (GO:0010035), reticulum endoplasmic stress (GO:0034976) and marked changes in proteins involved in the oxidation–reduction process (GO:00055114) with regulation of oxidative stress-induced intrinsic apoptotic signalling pathway (GO:1902175) (Figure 7). Differently and remarkably, in QM only, GO enrichment analysis pointed out a response to metal ion (GO:0010038) with positive regulation of proteolysis (GO:0045862). In this species, there is a notably greater number of altered cellular processes: response to oxidative stress (GO:0006979), glutathione metabolic process (GO:0006749), regulation of cell death (GO:0010941), regulation of transcription from RNA polymerase II promoter in response to stress (GO:0043618), post-transcriptional regulation of gene expression (GO:0010608), and cilium organisation (GO:0044782) (Figure 7).

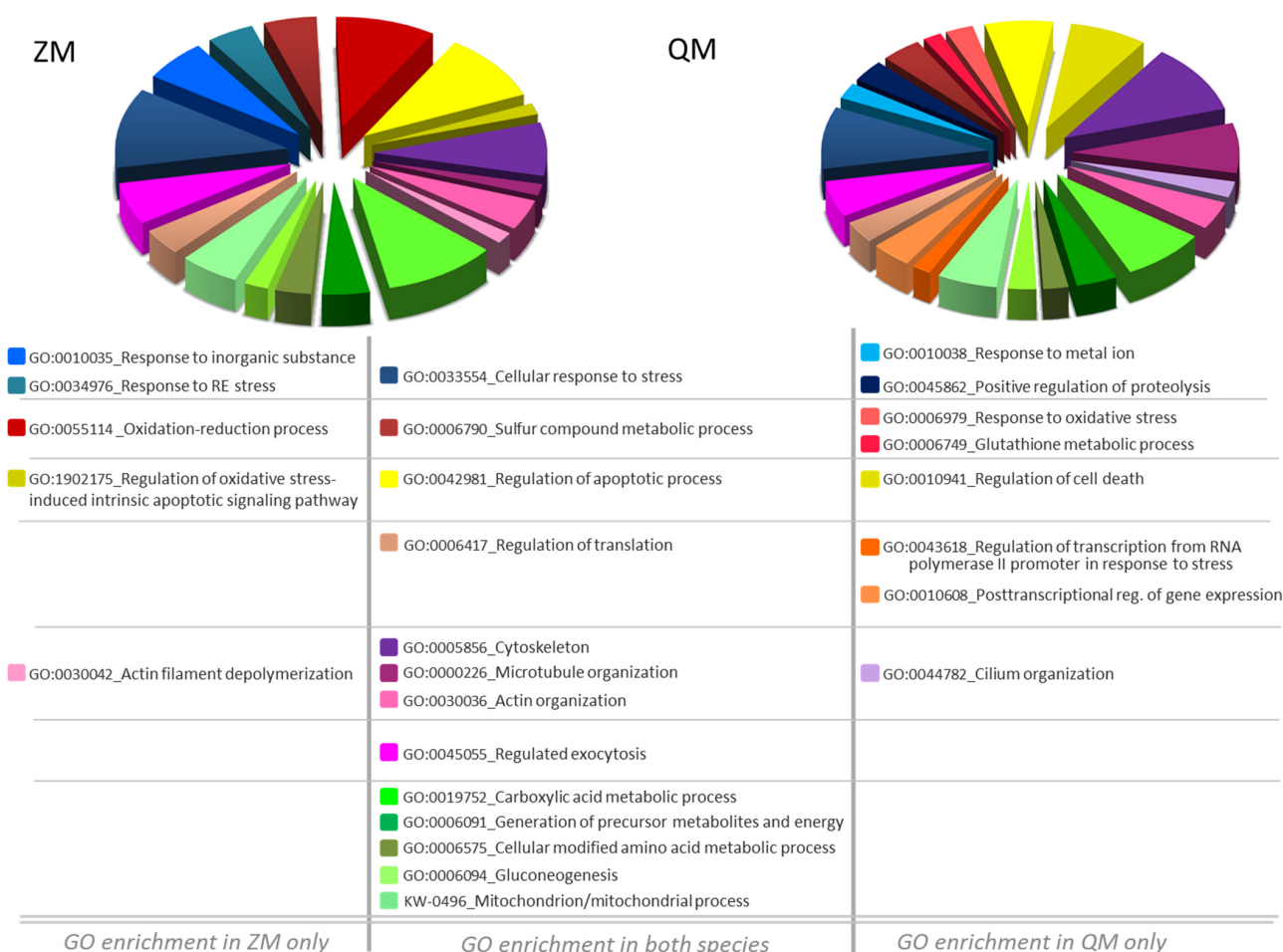


Figure 7. Pie Chart Diagram of GO biological process enrichment after *Dreissena* exposure to cadmium. Genome Ontology (GO) enrichment analysis of Cd induced DAPs-related biological processes. Allocation of biological processes is detailed in Table S4. Left, zebra mussel (ZM) and right, quagga mussel (QM).

4.3. Overlapping Modifications between ZM and QM

4.3.1. Chaperon, Folding, and Degradation

Components of the chaperone, processing, folding, and degradation category mediate the correct folding of newly synthesised proteins and the detoxification of damaged or misfolded ones [29,42]. Activation of the cell response to stress was detected in both species. Indeed, several HSPs underwent abundance modifications in either both species (Heat shock proteins 70, HSP70; mitochondrial Heat shock protein family D member 1, HSPD1) or in one of the two species (ZM: HSPB1, DNAJB11, HSP90AA1, HSP90B1, and QM: HSPA5; for details, see Tables 1B and S5), showing the set-up of a process to withstand cadmium-induced stress.

HSP70s play a critical role as protein chaperones, protecting the proteome from damages and cells from injury. They are involved in the folding of nascent or misfolded proteins, and in triggering the degradation of misfolded proteins if a proper structure cannot be restored. They also chaperone the association or dissociation of multi-protein complexes. Under oxidative stress, HSP70 additionally promotes the 20S proteasome-driven recycling of oxidatively damaged proteins [43,44].

HSPD1, alias hsp60 or 60 kDa heat shock protein, also displayed an increased abundance in both species. This chaperone is involved in the import of proteins into the mitochondrial matrix and, along with Hsp10, enables their correct folding. In case of mitochondrial stress, HSPD1 protects proteins from misfolding and promotes the proper

refolding of the unfolded peptides produced during stress [45]. The induction of a mitochondrial HSP response is consistent with the fact that mitochondria are known targets of cadmium [32,45–48].

A decrease in abundance of the beta subunit of prolyl 4-hydroxylase (P4HB) has been observed in both species. P4HB is the ER most abundant disulfide isomerase and is involved in the synthesis and rearrangement of disulfide bonds in nascent and misfolded proteins. Moreover, it may act as a molecular chaperone amid ER stress. This function is closely linked to its concentration. At high concentrations, P4HB prevents the aggregation of unfolded proteins, whereas at low concentrations, it promotes aggregation [49]. This may be relevant here as cadmium exposure decreases its abundance.

4.3.2. Antioxidant Response and Detoxification

Modification of antioxidant and biotransformation systems is a shared trait between ZM and QM. For instance, cadmium exposure elicited differential regulation of superoxide dismutases (SOD) and glutathione-S-transferases (GST) (ZM: SOD2; QM SOD1, GST, GSTP1; for details, see Table 1B and Table S5). This response was expected due to cadmium's properties and its ability to indirectly cause oxidative stress [22,24,31,40,50–60].

In particular, aldehyde dehydrogenase 1 family member A2 (ALDH1A2) abundance increased after cadmium exposure in both *Dreissena* species. Also known as retinal dehydrogenase 2, ALDH1A2 belongs to the aldehyde dehydrogenase family. ALDH1A2 converts retinaldehyde to retinoic acid, which plays a critical role in several cellular and molecular processes such as development, immunity, cell proliferation, or apoptosis by modulating retinoid signalling pathway. This cytosolic enzyme oxidises retinal and aliphatic aldehydes into the corresponding carboxylic acid, including 4-hydroxy-2-nonenal, a typical product of lipoperoxidation. ALDH1A2 could therefore reduce oxidative stress [61,62].

Furthermore, the GO term “sulphur compound metabolic process” is relevant to many DAPs in the antioxidant and detoxification category, e.g., previously cited GSTs, or glutaredoxin-3 (GLRX3) and bifunctional 3'-phosphoadenosine 5'-phosphosulfate synthase 1 (PAPSS1) for ZM and glutathione reductase (GSR) or glutathione synthetase (GSS) for QM (for details, see Table 1C, DAPs in bold). This is consistent with the presence of amino acids such as methionine or cysteine, or glutathione among the sulphur compounds. Moreover, sulfotransferase family 1A member 1 (SULT1A1) and cystathionine gamma-lyase (CTH) were upregulated by cadmium exposure. SULT1A1 is a sulfotransferase implicated in sulphate conjugation using 3'-phospho-5'-adenylyl sulphate as a sulphate donor. Sulfonation enhances the hydrophilicity of the resultant conjugate, facilitating excretion. Regarding CTH, this enzyme is responsible for catalysing the final step in cystathionine conversion to L-cysteine. Part of cysteine is used to synthesise glutathione, a key component in regulating the intracellular redox state. CTH has the ability to produce persulfides and polysulfides from cysteine resulting in products that may have multiple functions. By sulfhydrating the specific cysteine residue of target proteins, CTH can regulate their function. Additionally, persulfides and polysulfides produced in a non-specific manner are known to capture heavy metals such as cadmium, thereby facilitating their excretion. Finally, CTH can generate hydrogen sulphide (H₂S) from two cysteines. H₂S can prevent cell damage in the same way as persulfides while also acting as a gazotransmitter involved in several signalling pathways. Studies on frogs or chironoma showed an increase in CTH gene expression when exposed to heavy metals [38,39]. Furthermore, in myoblast cells, Zhang and colleagues proposed a pathway underlying the involvement of CTH and the produced H₂S in cell protection against Cd-induced cell death [63]. The increased abundance of cystathionine gamma-lyase is related to its critical position between glutathione synthesis and the integrated stress response, which helps to protect tissues from ER stress [64].

4.3.3. Translation Regulation

Control of protein synthesis is a key determinant of cell growth. Even slight modifications to the proteins involved in translation can alter protein synthesis, which in turn

can change the fate of a normal cell, leading it toward a tumorous or apoptotic state [65]. Several DAPs involved in regulating translation were identified in response to cadmium exposure: EIF5A, EEF2 (ZM), and EIF4A1, EIF4B (QM, for details, see Table 1 and Table S4). Additionally, two DAPs, namely eukaryotic translation initiation factor 3 subunit F (EIF3F) and proliferation-associated protein 2G4 (PA2G4), were detected in both species with increased abundance.

EIF3F is a noncore subunit of the eukaryotic translation initiation factor 3 complex, necessary for multiple phases of the protein synthesis initiation. The EIF3 complex is specifically involved in the translation of transcripts encoding proteins linked with cell proliferation and apoptosis. The composition of the EIF3 complex can differ, and variants exhibit cytosolic and/or nuclear localisation, suggesting moonlighting functions. The occurrence of EIF3F has been associated with the inhibition of translation and, in turn, proposed as a negative regulator of cell growth and proliferation [65]. Lastly, the EIF3 complex has been advanced as a potential biomarker of cadmium exposure in a cell or an organism [66].

By being involved in transcriptional and translational regulations as well as ribosome assembly, PA2G4 also plays a role in regulating cell growth and proliferation. For example, in the cytoplasm, PA2G4 associates with mature ribosomes and functions as an inhibitor of eukaryotic initiation factor 2 α (eIF2 α), thus blocking translation. In humans, two splicing variants with opposite functions have been described: the long PA2G4, which suppresses apoptosis and promotes cell growth, acting as an oncogene, and the short one, which functions as a tumour suppressor, promoting cell differentiation and suppressing proliferation. No such splicing has been described in *Dreissena* sp., and when we aligned the human and *Dreissena* sequences, it seemed likely that the two identified DAPs correspond to the full-length protein [67].

4.3.4. Energy Metabolism and Mitochondrial Alterations

Cadmium exposure affected carboxylic acid, amino acid metabolic and mitochondrial processes, including gluconeogenesis and generation of precursor metabolites and energy, all common to both species (for details, see Figure 3, Table 1D). Setting up molecular responses to combat metal toxicity requires energy. Organisms must increase their energy production by using the available carbohydrate reserves and by adjusting the function of several metabolic pathways [68]. In addition, proteins involved in metabolic pathways may themselves be targeted by cadmium, leading to additional perturbations.

No common DAPs were identified between species. The carboxylic acid metabolic process (GO:0019752) appeared to be the main response with regard to the use of carbohydrate reserve and modulation of metabolic pathways including the glycolytic and the pentose phosphate pathways, amino acids metabolism, gluconeogenesis, and within mitochondria, the TCA cycle and the synthesis of ATP via oxidative phosphorylation.

Examining the subcellular localisation of the identified DAPs reveals a noteworthy proportion located in the mitochondria. Cadmium is a well-documented mitochondrial toxin, accumulating within these organelles in vertebrate and invertebrate organisms, including bivalves [45–48]. This accumulation results in mitochondrial uncoupling, impaired ATP synthesis, and cellular energy imbalance [69–71]. Cadmium exposure may induce, in fine, mitochondrial swelling and provoke mitochondrial-dependent apoptosis [20,32].

4.3.5. Regulation of Apoptotic Process

The GO term “regulation of apoptotic process” is conserved between the two *Dreissena* species. As mentioned above, cadmium targets mitochondria and can induce apoptosis [27,30,72]. Interestingly, Joseph and colleagues reported an intricate connection between cadmium and apoptosis in cell culture studies. Cells surviving cadmium exposure could become resistant to cadmium-induced apoptosis. This could promote the survival and proliferation of cell with DNA damages, potentially leading to carcinogenic transformation [27]. These complex phenomena may explain the high representation of DAPs pertaining to the

GO term “regulation of apoptotic process” among the identified DAPs. This is especially true for those that are common to both species, including P4HB, ALDH1A2, and CTH, as well as for the PA2G4, and 60 kDa neurofilament protein (LMNA) presented in the next section regarding the cytoskeleton.

4.3.6. Cytoskeleton Modifications

Cadmium is a well-known stressor of the cytoskeleton, resulting in oxidative damage to its components and the disruption of its organisation [20,24,47,73–81].

In this study, a significant number of DAPs corresponding to components of the cytoskeleton (ZM: 24.7%; QM: 32.4%) were identified. These are mainly elements associated with microtubules and the beta and alpha subunits of tubulin itself. In both species, some identified DAPs exhibited much lower molecular mass than expected, suggesting fragmentation of alpha and beta tubulin subunits, filamin (FLNA), or LMNA. Regarding LMNA, in a proteomic study undertaken on freshwater mollusk *Lymnaea stagnalis* to investigate the molecular effects of nerve lesion, Perlson and collaborators identified cleavage products of intermediate filaments termed retrograde protein of 51 kDa (RGP51) which may perform both structural and signalling functions in retrograde injury signalling after cytoskeleton collapse [82]. Comparison of the MS/MS files indicated that 55 kDa LMNA could be consistent with the RGP51 sequence. In cadmium-exposed mussels, cleavages and modifications of intermediate filament abundance may participate to such a mechanism, i.e., rearrangement of cytoskeleton to redirect cell molecular trafficking under toxic pressure.

4.3.7. Exocytosis

Many DAPs involved in cellular trafficking, membrane endocytosis, and exocytosis were detected (16 for ZM, 17 for QM) with the major vault protein (MVP) TUBB, FLNA, and LMNA, in common. Interestingly, MVP was detected with a decreased abundance in both species. Major vault proteins are the main components of Vault ribonucleoparticles. These barrel-shaped structures with an internal cavity participate in nucleo-cytoplasmic trafficking and can shuttle between the nucleoplasm and the cytoplasm even though Vaults are mainly cytosolic. Vaults act as scaffolds for proteins involved in signal transduction in multiple kinase signalling pathways [83]. Vaults can export DNA-damaging drugs, and their connection with multidrug resistance in cancer through the exocytosis of drugs has been established [83]. Moreover, MVP has been discovered on the surface of cancer cells, unlike in normal cells. It is believed that this extracellular variant is linked with cancer progression [83]. In the context of our findings, it is worth noting that MVP is cytoprotective, and downregulation of MVP has been demonstrated to increase sensitivity to cell death [84].

As a conclusion, the cellular-level disruption of the cytoskeleton and trafficking can be put into perspective with branchial physiology. Several histological studies have explored the effects of cadmium on bivalve gills. The presence of cadmium-rich inclusions, structural and functional changes in membrane trafficking, increased exocytosis linked with a greater number of mucus cells, hyperplasia of the gill lamellae, loss of the lateral cilia that hold the lamellae together, rupture of the endothelial cells, and even necrosis are among the toxic effects of cadmium [85].

4.4. Focus on Some Species-Specific Modifications

4.4.1. DAPs That Display Common Identity but Opposite Direction of Variation

In our study, several proteins exhibited an increase in abundance in ZM and a decrease in QM, i.e., the far upstream element-binding protein 1 (FUBP1), the ATP-dependent RNA helicase (DDX3X), and the spermatogenesis associated 18 (SPATA18).

FUBP1 is a single-stranded DNA-binding protein that binds to multiple DNA elements, including the far upstream element (FUSE). FBP1 interacts with p53, functions as a regulator of p53-regulatory proteins, and suppresses p53 transactivation activity under

radiation-induced cellular stress [86]. It also regulates the c-myc proto-oncogene, a master regulator of cell proliferation, differentiation, and apoptosis. FUBP1 regulates c-myc expression by binding to a single-stranded far-upstream element (FUSE) upstream of the c-myc promoter [87]. In ZM, the FUBP1 increase suggests a modulation via c-myc. However, in QM, we also identified a DAP capable of modifying c-myc: a short ENO highly similar to the c-myc promoter-binding protein-1 isoform (MBP-1), which shows a decreased abundance. MBP-1 binds to the c-myc transcription factor and suppresses its activity [19]. These observations are consistent with the activation of the c-jun Nterminal kinase (JNK) pathway under cadmium stress, resulting in increased expression of c-fos, c-jun, and c-myc [30]. In blood clam *Tegillarca granosa* gills, up-regulation of c-myc has also been observed after cadmium exposure, suggesting that c-myc regulates cadmium-induced stress response and detoxification in the bivalves [88].

DDX3X belongs to the DEAD-box helicase family and is involved in many aspects of RNA biology. Its functions include the transcription regulation of certain genes involved in cell cycle regulation, signalling pathways, or cell adhesion. It is also implicated in RNA splicing and export to the cytoplasm. Finally, DDX3X is involved in the initiation of both cap-dependent and cap-independent translation. In cancer cells, DDX3X was shown to globally repress protein synthesis while fostering the translation of specific RNAs by binding to the eIF4F complex. In the context of ER stress, DDX3X is required for the translation of ATF4, a key transcription factor in the integrated stress response. During cell stress, DDX3X plays a pivotal role in determining cell fate, as it is involved in two competing processes: it either contributes to the assembly of stress granules, which provide cytoprotection, or it can interact with NLRP3 (for NACHT, LRR and PYD domains containing protein 3) and trigger the inflammasome activation, leading to pyroptosis. The availability of DDX3X for either process acts as a central regulator of the balance between cell survival and death [89].

SPATA18, also known as the mitochondria-eating protein, is a key regulator of mitochondrial quality responsible for repairing or degrading damaged mitochondria. Its transcription is positively regulated by p53. When mitochondrial damage occurs, a process involving SPATA18 called mitochondrial eating protein-induced accumulation of lysosome-like organelles within mitochondria (MALM) is activated [90]. SPATA18 plays an essential role in MALM by opening a pore that enables lysosomal proteins to enter the mitochondrial matrix without altering the mitochondrial structure. The oxidised proteins are subsequently degraded by lysosomal hydrolases, resulting in increased ATP production. SPATA18 also participate in the mitophagy of damaged mitochondria. Recent studies have shown that SPATA18 silencing impedes mitophagy induction, resulting in the persistence of damaged mitochondria [91]. The opposite abundance variations of this protein suggest that mitochondrial repair processes were activated in ZM but not in QM.

Conversely, increases in proteins were observed in QM and decreases were noted in ZM, such as the cytoplasmic tryptophanyl-tRNA synthetase cytoplasmic (WARS1), manganese-dependent cytosolic non-specific dipeptidase (CNDP2), calponin 3 (CCN3) and maleylacetoacetate isomerase (GSTZ1).

WARS1 catalyses the ligation of tryptophan to its ARNt. In humans, WARS1 expression is induced by interferon γ and it is implicated in multiple physiopathological processes such as immunity or cancer [92]. Little is known about non-canonical functions of WARS in invertebrates, although modulation of WARS1 has already been described in scallops under stress [93]. Its increase in QM may reflect inflammation.

CNDP2 is ubiquitously expressed and highly conserved. CNDP2 exhibits a broad substrate specificity with a preference for cysteinyl-glycine, an intermediate metabolite in glutathione metabolism. In addition, in gastric cancer, CNDP2 may activate the p38 and JNK MAPK pathways, leading to cell apoptosis when highly expressed, or the ERK MAPK pathway, promoting cell proliferation when expressed at a low level [94]. If bivalve CNDP2 functions similarly, its reduction in ZM would suggest greater resistance to cad-

mium exposure, while its low abundance in QM would indicate an imbalance in favour of apoptosis.

CCN3 is a thin filament-associated protein implicated in actin bundling and actin filament dynamics, and it also contributes to actin filament stability. Decreases in calponin abundance have been documented in green mussels exposed to cadmium [22]. The opposite variation between ZM and QM is consistent with the distinct modifications of the actin cytoskeleton observed in these two species.

GSTZ1, also known as soluble glutathione S-transferase, is a multifunctional enzyme. Its main activity is linked to the phenylalanine/tyrosine degradation pathway with the ability to convert maleylacetoacetate into fumarylacetoacetate. GSTZ1, as a biotransformation enzyme, can also conjugate GSH, although this activity is deemed minor. A third function, i.e., glutathione peroxidase, has been described. GSTZ1 is considered as a sign of cadmium-induced stress [45]. The observed abundance variations, regardless of their direction, support GSTZ1 as a potential biomarker.

4.4.2. ZM-Specific Modifications

ZM-specific proteome modifications in response to cadmium exposure can be illustrated by two GO terms, i.e., “Response to endoplasmic reticulum stress” and “Actin filament depolymerisation”. The GO term Response to endoplasmic reticulum stress was evidenced only in ZM with a group of 7 DAPs including dnaJ homolog subfamily B member 11 (DNAJB11), endoplasmin (HSP90B1), small heat shock protein p36 (HSPB1), transitional endoplasmic reticulum ATPase (VCP), and ubiquitin-fold modifier-conjugating enzyme 1 (UFC1). In addition to its ability to bind to thiol groups of proteins, cadmium can mimic calcium and interfere with its signalling pathway [20]. Disruption of calcium homeostasis in the endoplasmic reticulum can cause protein misfolding and result in ER stress [95]. Cellular response to stress is present in both species, but ZMs seem to develop stronger defence mechanisms to face cadmium.

As previously mentioned, actin is a target of oxidative stress resulting from cadmium exposure [73,74]. The cytoskeleton may deeply affect the modified dynamics of actin polymerisation/depolymerisation and potentially disrupt the focal adhesion contacts [20]. In ZM, several DAPs are actin-related proteins, including twinfilin actin binding protein 1 (TWF1), cofilin-1 (CFL1), and WD repeat-containing protein 1 (WDR1). They all play a role in cytoskeletal organisation in epithelial cells such as gills and exhibit an increased abundance in response to cadmium. TWF1 and CFL1 are actin-binding proteins that inhibit actin polymerisation. WDR1 alias actin-interacting protein 1 is regulator of actin-dependent processes increasing the stability of cortical actin in a calcium-dependent manner and, conversely, the disassembly of actin filaments in conjunction with cofilin family proteins [76]. Lewinska and colleagues showed that c-myc activation promotes cofilin-mediated remodelling of the actin cytoskeleton in response to oxidative DNA damage [96]. In ZM, increased abundances of TWF1 and CFL1 can be related to aforementioned modifications of c-myc regulation, implying that repair mechanisms are activated.

4.4.3. QM-Specific Modifications

As already mentioned, in QM only, GO enrichment analysis indicated a response to metal ion with positive regulation of proteolysis and a notably greater number of altered cellular processes including regulation of cell death and cilium organisation (Figure 3, Table S4).

Cytoskeletal modifications are more pronounced in QM, with a larger number of modified proteins belonging to the microtubule organisation and specifically to the organisation of ciliated epithelial structures. These observations imply more significant effects of cadmium on the QM gills, resulting in marked histological and physiological alterations. In gills of the clam, *Meretrix meretrix*, cadmium leads to mitochondria-mediated apoptosis with induction of caspases and disorganised ciliary orientation with impairment of microtubules [48]. Consistent with these protein alterations, changes in the proteasome are also specifically observed in QM. The 26S proteasome is involved in the ATP-dependent

degradation of ubiquitinated proteins. This multiprotein complex is formed by association of the 20S core particle with the 19S regulatory particle. It plays a key role in the maintenance of protein homeostasis by removing misfolded or damaged proteins, which could impair cellular functions, and by removing proteins whose functions are no longer required [44]. Under oxidative stress, damaged protein accumulation in the cell could partly be removed by proteasome activity. In QM only, several DAPs have been identified as subunits of the proteasome: 26S proteasome non-ATPase regulatory subunit 14 (PSMD14), 26S proteasome regulatory subunit 10B (PSMC6), proteasome subunits alpha type-2 (PSMA2), and proteasome subunit alpha type-4 (PSMA4). The PSMD14 alias Rpn11 is a deubiquitinating enzyme that belongs to the metalloenzyme JAMM family. PSMD14 is a deubiquitinating enzyme for proteins directed towards the proteasome. The enzyme is a metalloprotease that contains a Jab1/MPN metalloenzyme domain motif (JAMM) linked to the zinc ion, so cadmium may impair the zinc–JAMM interaction. PSMD14 plays a key role in maintaining proper mitochondrial function. Furthermore, PSMC6 is a member of the AAA proteins (for ATPases associated with diverse cellular activities proteins) and plays a role in deubiquitylation by unfolding polyubiquitinated proteins. This allows for their entrance into the catalytic zone of the proteasome, following DUB polyubiquitin chain cleavage. PSMA2 and PSMA4 are components of the 20S core proteasome complex. Oxidative stress favours the disassembly of the 26S proteasome complex into 20S and 19S particles and the degradation of oxidised proteins by the 20S core. Consequently, the 20S proteasome appears to be the major machinery involved in degradation of oxidised proteins in response to oxidative stress, even if degradation of damaged proteins can still occur by ubiquitin/ATP-dependent activity of the 26S proteasome [44]. Finally, this observation indicates that cadmium induces more proteolytic processes in QM than in ZM, as also supported by the GO enrichment positive regulation of proteolysis (GO:0045862) in QM. Significant enrichment of the cellular proteolysis process was also observed in clams following exposure to 50 $\mu\text{g}\cdot\text{L}^{-1}$ cadmium [24].

5. Synthesis

Overall, cadmium exposure in both species resulted in the development of resistance mechanisms to cadmium-induced apoptosis (Figure 8). Hence, cellular stress response activation was detected in both species. Regarding protein synthesis, we observed the induction of proteins involved in negative regulation of translation such as PA2G4 and EIF3F; the latter has already been described as a potential biomarker of cadmium exposure [66]. In parallel, marked HSPD1 and HSP70 increases were detected, indicating the activation of folding and degradation pathways. Moreover, a decreased abundance of P4HB, which promotes aggregation of unfolded proteins at low levels, is another indicator of ER-stress observed in both species. Common responses also relied on a specific antioxidant cell response against Cd-induced cell death, marked by increased levels of ALDH1A2, SULT1A, and CTH. CTH could be proposed as a potential biomarker of cadmium exposure due to its involvement in the production of H_2S , which helps to prevent cell damage by capturing heavy metals. As expected, both species displayed changes in protein abundances implicated in metabolic pathways, including glycolytic and pentose phosphate pathways, amino acid metabolism, gluconeogenesis, TCA cycle, and oxidative phosphorylation. It is likely that these changes are related to an increased demand for energy.

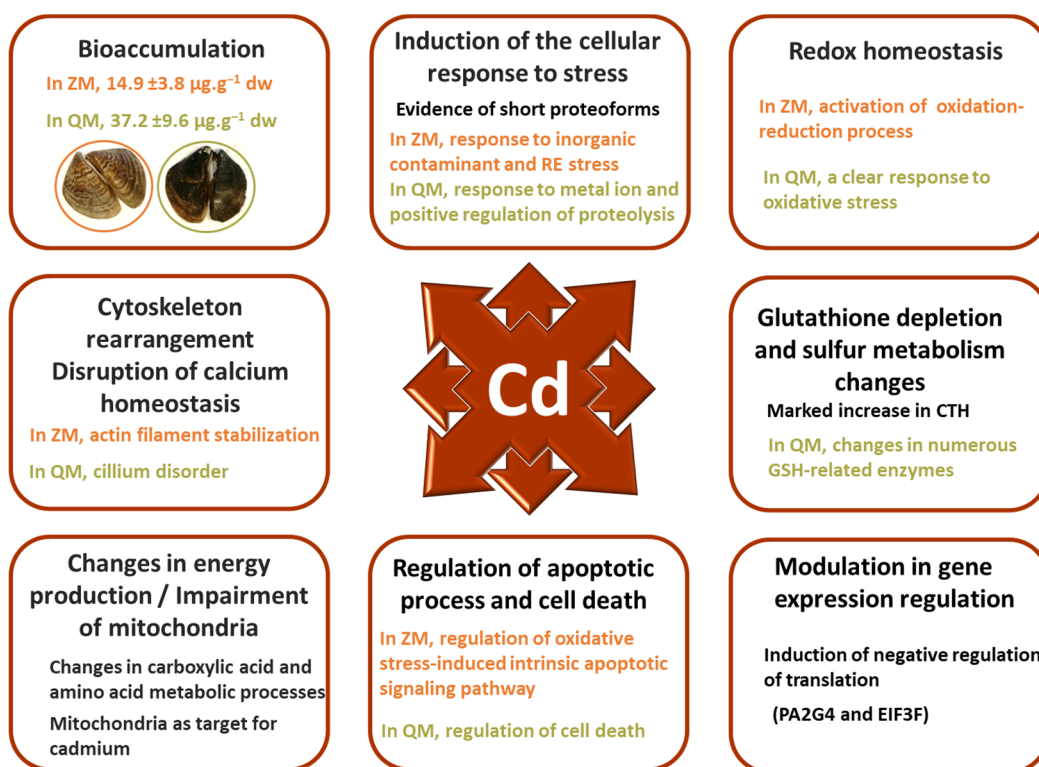


Figure 8. Modulations of *Dreissena* gill proteomes are consistent with Cd exposure but partly differ reflecting species-specific cellular strategies in fighting homeostasis rupture.

Cadmium toxicity mainly affects the mitochondria, cytoskeleton, and calcium signalling, leading to oxidative stress. The modifications observed in the sister species are largely linked to these deleterious effects, but species-specific responses were detected. For example, the non-specific antioxidant response was stronger in ZM compared to QM. There is more evidence of cytoskeleton rearrangement and increases in cellular trafficking and membrane exocytosis in QM compared to ZM. These changes may be associated with more gill cilia damage in QM. The results also suggest an activation of the c-myc regulatory pathway in both species, although mediated differently. In QM, a decrease in a short ENO proteoform highly similar to the c-myc promoter-binding protein-1 isoform (MBP-1) was observed. In ZM, increased abundances of FUBP1, TWF1, and CFL1 indicate cofilin-mediated remodelling of the actin cytoskeleton promoted by c-myc activation in response to oxidative DNA damage. Opposite abundance variations of some proteins, including SPATA18, CNBP2, WARS1, CCN3 and GSTZ1, suggest a better activation of mitochondrial repair processes and a greater resistance to cadmium exposure in ZM than in QM, where inflammation and apoptotic processes appeared more evident. It should be noted that GSTZ1 variation is considered as a sign of cadmium-induced stress.

Interestingly, proteoforms with molecular weights significantly lower than those of the canonical proteins were observed. The presence of these proteoforms is more prominent in QM than in ZM. The question of a non-canonical function is raised for some of these short proteoforms.

Taken together, the findings of this work are in accordance with prior studies indicating that ZM populations have a greater ability to activate their defence mechanisms when facing contamination, while QM appear less able to adapt to coping with the contamination they are exposed to [97]. It is also noteworthy that biomarker assessment following a 7-day cadmium exposure ($10 \mu\text{g}\cdot\text{L}^{-1}$) revealed no response in QM while ZM showed variations [8]. This could be associated to the inability of QM to induce functional defence mechanisms rather than to a resistance to contamination. Indeed, similar responses were observed following Ni short-term exposure, and they were finally related to a lower toler-

ance of QM [98]. Cadmium can trigger both autophagy and apoptosis, thereby impacting cell viability [47,99]. The difference in cadmium tolerance between the two species may be explained by the formation of apoptotic degradosome vesicles in QM and a potential autophagic response in ZM. Finally, QMs appear to be less tolerant to high stress levels than ZMs, which display the ability to activate distinct cellular strategies to cope with homeostasis disruption in the event of contamination [98].

This work is in line with the known pleiotropic effects of cadmium. However, it also highlights species-specific responses with proteoforms identified solely in QM or ZM, or common proteoform exhibiting opposite variations of abundances. It would be of interest to further compare QM and ZM responses to heavy metal through multi-omics approaches.

6. Conclusions

A classic pollutant was used to highlight the difference in stress response between two mussel species used as sentinel in freshwater biomonitoring. Cadmium treatment induced significant proteomic alterations in the gills of quagga and zebra mussels that are consistent with the known effects of cadmium exposure. Overall, QM displayed higher cadmium accumulation and marked alterations in the gill proteome compared to ZM. Although sharing common features, the proteomic modification profiles exhibited significant differences. In particular, QM and ZM react to cadmium by implementing distinct defence and survival responses. This reinforces our view that the two species are not interchangeable in environmental biomonitoring, emphasising the importance of precise species identification.

Supplementary Materials: The following are available online at <https://www.mdpi.com/article/10.3390/proteomes12020010/s1>, Table S1: MS/MS identification of zebra mussel differentially abundant proteoforms after cadmium exposure. Table S2: MS/MS identification of quagga mussel differentially abundant proteoforms after cadmium exposure. Table S3: Colour version of Table 1 including observed MW and pI. Table S4: Gene Ontology Biological Process enrichment in zebra and quagga mussel gills after cadmium exposure. Table S5: Short Summary of protein functions extracts from online database annotations [19–112]. Figure S1: Water physicochemical parameters during the 7-day of cadmium exposure. Figure S2: images of selected 2DE gels of Zebra Mussel gill proteome. Figure S3: images of selected 2DE gels of Quagga Mussel gill proteome. Figure S4: Distribution of ZM_DAPs based on main GO terms in zebra mussel (ZM) gills after cadmium exposure. Figure S5: Distribution of QM_DAPs based on main GO terms in quagga mussel (QM) gills after cadmium exposure. Figure S6: Evidence of cytoskeleton short proteoforms revealed by cadmium exposure. Figure S7: Comparison of HSP70 proteoforms in quagga mussel (QM).

Author Contributions: Conceptualization, F.B., B.R., S.P.-D. and E.D.; Formal analysis, A.L.S., R.P., A.T. and S.D.; Investigation, F.B., A.T., S.O., A.P., P.C., L.D., D.V., B.R. and E.D.; Project administration, F.B., S.P.-D., S.D., A.T., B.R. and E.D.; Supervision, F.B. and B.R.; Writing—original draft, F.B. and B.R.; Writing—review and editing, F.B., E.D., A.T., S.D., P.C., F.L., S.P.-D., S.D., D.V., F.L.F. and B.R.; Funding acquisition, E.D. All authors have read and agreed to the published version of the manuscript.

Funding: This research was funded by the Rovaltain Foundation for scientific cooperation (PolQua project, AO RTE2015) and was supported by FR CNRS 3730 SCALE. Aimie Le Saux was a recipient of a PhD grant from the French Ministry for Research.

Institutional Review Board Statement: Not applicable. Experiments on non-cephalopod invertebrates are not subject to authorisation by the Institutional Review Board Statement in European Union.

Informed Consent Statement: Not applicable.

Data Availability Statement: The data are public on the figshare.com website: https://figshare.com/projects/Cadmium_highlights_common_and_specific_responses_of_the_two_dreissenid_species_Dreissena_polymorpha_and_Dreissena_rostri-formis_bugensis/198700 (accessed on 18 March 2024).

Acknowledgments: We thank Morgane Lebreton and Odile Dedourge-Geffard for their help in mussel sampling, and Damien Maclard for his bioinformatics assistance.

Conflicts of Interest: The authors declare no conflict of interest. The funders had no role in the design of the study; in the collection, analyses, or interpretation of data; in the writing of the manuscript; or in the decision to publish the results.

References

1. Binelli, A.; Della Torre, C.; Parolin, M. Does zebra mussel (*Dreissena polymorpha*) represent the freshwater counterpart of *Mytilus* in ecotoxicological studies? A critical review. *Environ. Pollut.* **2015**, *196*, 386–403. [[CrossRef](#)] [[PubMed](#)]
2. Mills, E.; Rosenberg, G.; Spidle, A.P.; Ludyanskiy, M.; Pligin, Y.; May, B. A review of the biology and ecology of the quagga mussel (*Dreissena bugensis*), a second species of freshwater Dreissenid introduced to North America. *Amer. Zool.* **1996**, *36*, 271–286. [[CrossRef](#)]
3. Bij de Vaate, A.; Beisel, J.-N. Range expansion of the quagga mussel *Dreissena rostriformis bugensis* (Andrusov, 1897) in Western Europe: First observation from France. *Aquat. Invasions* **2011**, *6*, S71–S74. [[CrossRef](#)]
4. Karatayev, A.Y.; Burlakova, L.E. What we know and don't know about the invasive zebra (*Dreissena polymorpha*) and quagga (*Dreissena rostriformis bugensis*) mussels. *Hydrobiologia* **2022**, *13*, 1–74. [[CrossRef](#)]
5. Schäfer, S.; Hamer, B.; Treursić, B.; Möhlenkamp, C.; Korlević, M.; Reifferscheid, G.; Claus, E. Comparison of bioaccumulation and biomarker responses in *Dreissena polymorpha* and *D. bugensis* after exposure to resuspended sediments. *Arch. Environ. Contam. Toxicol.* **2012**, *62*, 614–627. [[CrossRef](#)] [[PubMed](#)]
6. Kerambrun, E.; Delahaut, L.; Geffard, A.; David, E. Differentiation of sympatric zebra and quagga mussels in ecotoxicological studies: A comparison of morphometric data, gene expression, and body metal concentrations. *Ecotoxicol. Environ. Saf.* **2018**, *154*, 321–328. [[CrossRef](#)] [[PubMed](#)]
7. Evariste, L.; David, E.; Cloutier, P.-L.; Brousseau, P.; Auffret, M.; Desrosiers, M.; Groleau, P.E.; Fournier, M.; Betoulle, S. Field biomonitoring using the zebra mussel *Dreissena polymorpha* and the quagga mussel *Dreissena bugensis* following immunotoxic responses. Is there a need to separate the two species? *Environ. Pollut.* **2018**, *238*, 706–716. [[CrossRef](#)] [[PubMed](#)]
8. Potet, M.; Devin, S.; Pain-Devin, S.; Rousselle, P.; Giambérini, L. Integrated multi-biomarker responses in two dreissenid species following metal and thermal cross-stress. *Environ. Pollut.* **2016**, *218*, 39–49. [[CrossRef](#)] [[PubMed](#)]
9. Louis, F.; Devin, S.; Giambérini, L.; Potet, M.; David, E.; Pain-Devin, S. Energy allocation in two dreissenid species under metal stress. *Environ. Pollut.* **2019**, *245*, 889–897. [[CrossRef](#)]
10. Farkas, A.; Ács, A.; Vehovszky, Á.; Falfusynska, H.; Stoliar, O.; Specziár, A.; Györi, J. Interspecies comparison of selected pollution biomarkers in dreissenid spp. inhabiting pristine and moderately polluted sites. *Sci. Total Environ.* **2017**, *599–600*, 760–770. [[CrossRef](#)]
11. Zhang, H.; Reynolds, M. Cadmium exposure in living organisms: A short review. *Sci. Total Environ.* **2019**, *678*, 761–767. [[CrossRef](#)] [[PubMed](#)]
12. Zhao, X.-M.; Yao, L.-A.; Ma, Q.-L.; Zhou, G.-J.; Li Wang, L.; Fang, Q.-L.; Xu, Z.-C. Distribution and ecological risk assessment of cadmium in water and sediment in Longjiang River, China: Implication on water quality management after pollution accident. *Chemosphere* **2018**, *194*, 107–116. [[CrossRef](#)] [[PubMed](#)]
13. Perera, P.A.C.T.; Sundarabharathy, T.V.; Sivananthawerl, T.; Kodithuwakku, S.P.; Edirisinghe, U. Arsenic and Cadmium Contamination in Water, Sediments and Fish is a Consequence of Paddy Cultivation: Evidence of River Pollution in Sri Lanka. *Achiev. Life Sci.* **2016**, *10*, 144–160. [[CrossRef](#)]
14. Amiard, J.-C.; Pineau, A.; Boiteau, H.L.; Métayer, C.; Amiard-Triquet, C. Application of atomic absorption spectrometry using Zeeman effect to the determination of eight trace elements (Ag, Cd, Cr, Cu, Mn, Ni, Pb et Se) in biological materials. *Water Res.* **1987**, *21*, 696–697. [[CrossRef](#)]
15. Péden, R.; Rocher, B.; Chan, P.; Vaudry, D.; Poret, A.; Olivier, S.; Le Foll, F.; Bultelle, F. Consequences of acclimation on the resistance to acute thermal stress: Proteomic focus on mussels from pristine site. *Mar. Environ. Res.* **2016**, *121*, 64–73. [[CrossRef](#)] [[PubMed](#)]
16. Péden, R.; Poupin, P.; Sohm, B.; Flayac, J.; Giambérini, L.; Klopp, C.; Louis, F.; Pain-Devin, S.; Potet, M.; Serre, R.-F.; et al. Environmental Transcriptomes of Invasive *Dreissena*, a Model Species in Ecotoxicology and Invasion Biology. *Sci. Data* **2019**, *6*, 234. [[CrossRef](#)] [[PubMed](#)]
17. Szklarczyk, D.; Gable, A.L.; Lyon, D.; Junge, A.; Wyder, S.; Huerta-Cepas, J.; Simonovic, M.; Doncheva, N.T.; Morris, J.H.; Bork, P.; et al. STRING v11: Protein–protein association networks with increased coverage, supporting functional discovery in genome-wide experimental datasets. *Nucleic Acids Res.* **2019**, *47*, D607–D613. [[CrossRef](#)] [[PubMed](#)]
18. Roseman, E.F.; Mills, E.L.; Rutzke, M.; Gutenmann, W.H.; Lisk, D.J. Absorption of cadmium from water by north american zebra and quagga mussels (bivalvia: Dreissenidae). *Chemosphere* **1994**, *28*, 737–743. [[CrossRef](#)]
19. Zhang, K.; Zhang, J.; Ding, N.; Zellmer, L.; Zhao, Y.; Liu, S.; Liao, D.J. ACTB and GAPDH appear at multiple SDS-PAGE positions, thus not suitable as reference genes for determining protein loading in techniques like Western blotting. *Open Life Sci.* **2021**, *16*, 1278–1292. [[CrossRef](#)]
20. Choong, G.; Liu, Y.; Templeton, D.M. Interplay of calcium and cadmium in mediating cadmium toxicity. *Chem. Biol. Interac.* **2014**, *211*, 54–65. [[CrossRef](#)]
21. Péden, R.; Rocher, B.; Chan, P.; Vaudry, D.; Poret, A.; Olivier, S.; Le Foll, F.; Bultelle, F. Highly polluted life history and acute heat stress, a hazardous mix for blue mussels. *Mar. Pollut. Bull.* **2018**, *135*, 594–606. [[CrossRef](#)] [[PubMed](#)]

22. Leung, P.T.Y.; Wang, Y.; Mak, S.S.T.; Ng, W.C.; Leung, K.M.Y. Differential proteomic responses in hepatopancreas and adductor muscles of the green-lipped mussel *Perna viridis* to stresses induced by cadmium and hydrogen peroxide. *Aquat. Tox.* **2011**, *105*, 49–61. [[CrossRef](#)]
23. Zheng, X.; Gao, Y.; Li, W.; Wang, S. iTRAQ-based quantitative proteomic analysis identified Eno1 as a cadmium stress response gene in *Propiloscerus akamusi* (Tokunaga) hemolymph. *Ecotoxicol. Environ. Saf.* **2018**, *165*, 126–135. [[CrossRef](#)] [[PubMed](#)]
24. Huang, Y.; Dai, Y.; Li, M.; Guo, L.; Cao, C.; Huang, Y.; Ma, R.; Qiu, S.; Su, X.; Zhong, K.; et al. Exposure to cadmium induces neuroinflammation and impairs ciliogenesis in hESC-derived 3D cerebral organoids. *Sci. Total Environ.* **2021**, *797*, 149043. [[CrossRef](#)]
25. Zhang, X.; Li, F.; Ji, C.; Wu, H. Toxicological mechanism of cadmium in the clam *Ruditapes philippinarum* using combined ionic, metabolomic and transcriptomic analyses. *Environ. Pollut.* **2023**, *323*, 121286. [[CrossRef](#)]
26. Zhan, X.; Li, B.; Zhan, X.; Schlüter, H.; Jungblut, P.R.; Coorsen, J.R. Innovating the concept and practice of Two-Dimensional Gel Electrophoresis in the analysis of proteomes at the proteoform level. *Proteomes* **2019**, *7*, 36. [[CrossRef](#)]
27. Joseph, P. Mechanisms of cadmium carcinogenesis. *Toxicol. Appl. Pharmacol.* **2009**, *238*, 272–279. [[CrossRef](#)] [[PubMed](#)]
28. Thévenod, F. Cadmium and cellular signaling cascades: To be or not to be? *Toxicol. Appl. Pharmacol.* **2009**, *238*, 221–239. [[CrossRef](#)]
29. Tamás, M.; Fauvet, B.; Christen, P.; Goloubinoff, P. Misfolding and aggregation of nascent proteins: A novel mode of toxic cadmium action in vivo. *Curr. Genet.* **2018**, *64*, 177–181. [[CrossRef](#)]
30. Đukic-Cosic, D.; Baralic, K.; Javorac, D.; Djordjevic, A.B.; Bulat, Z. An overview of molecular mechanisms in cadmium toxicity. *Curr. Opin. Toxicol.* **2020**, *19*, 56–62. [[CrossRef](#)]
31. Le Saux, A.; David, E.; Betoulle, S.; Bultelle, F.; Rocher, B.; Barjhoux, I.; Cosio, C. New insights into cellular impacts of metals in aquatic animals. *Environments* **2020**, *7*, 46. [[CrossRef](#)]
32. Lee, W.-K.; Thévenod, F. Cell organelles as targets of mammalian cadmium toxicity. *Arch. Toxicol.* **2020**, *94*, 1017–1049. [[CrossRef](#)]
33. Si, Y.-X.; Lee, J.; Zhao, F.; Yin, S.-J.; Park, Y.-D.; Qian, G.-Y. Effects of cadmium on the cuttlefish *Sepia pharaonis*' arginine kinase: Unfolding kinetics integrated with computational simulations. *J. Biomol. Struct. Dyn.* **2015**, *34*, 1763–1777. [[CrossRef](#)] [[PubMed](#)]
34. Lin, C.-H.; Yeh, P.-L.; Lee, T.-H. Ionic and amino acid regulation in hard clam (*Meretrix lusoria*) in response to salinity challenges. *Front. Physiol.* **2016**, *7*, 368. [[CrossRef](#)] [[PubMed](#)]
35. Harcet, M.; Perina, D.; Pleše, B. Opine Dehydrogenases in Marine Invertebrates. *Biochem. Genet.* **2013**, *51*, 666–676. [[CrossRef](#)] [[PubMed](#)]
36. Han, G.; Zhang, S.; Dong, Y. Anaerobic metabolism and thermal tolerance: The importance of opine pathways on survival of a gastropod after cardiac dysfunction. *Integr. Zool.* **2016**, *12*, 361–370. [[CrossRef](#)] [[PubMed](#)]
37. Ivanina, A.V.; Cherkasov, A.S.; Sokolova, I. Effects of cadmium on cellular protein and glutathione synthesis and expression of stress proteins in eastern oysters, *Crassostrea virginica* Gmelin. *J. Exp. Biol.* **2008**, *211*, 577–586. [[CrossRef](#)]
38. Jeppe, K.J.; Carew, M.E.; Long, S.; Lee, S.F.; Pettigrove, V.; Hoffmann, A.A. Genes involved in cysteine metabolism of *Chironomus tepperi* are regulated differently by copper and by cadmium. *Comp. Biochem. Physiol. C* **2014**, *162*, 1–6. [[CrossRef](#)]
39. Kaczor-Kaminska, M.; Sura, P.; Wróbel, M. Multidirectional changes in parameters related to sulfur metabolism in frog tissues exposed to heavy metal-related stress. *Biomolecules* **2020**, *10*, 574. [[CrossRef](#)]
40. Xia, L.; Chen, S.; Dahms, H.-U.; Ying, X.; Peng, X. Cadmium induced oxidative damage and apoptosis in the hepatopancreas of *Meretrix meretrix*. *Ecotoxicology* **2016**, *25*, 959–969. [[CrossRef](#)]
41. Huang, Y.; Tang, H.; Jin, J.; Fan, M.; Chang, A.K.; Ying, X. Effects of waterborne cadmium exposure on its internal distribution in *Meretrix meretrix* and detoxification by metallothionein and antioxidant enzymes. *Front. Mar. Sci.* **2020**, *7*, 502. [[CrossRef](#)]
42. Qiu, X.-B.; Shao, Y.-M.; Miao, S.; Wang, L. The diversity of the DnaJ/Hsp40 family, the crucial partners for Hsp70 chaperones. *Cell. Mol. Life Sci.* **2006**, *63*, 2560–2570. [[CrossRef](#)] [[PubMed](#)]
43. Reeg, S.; Jung, T.; Castro, J.P.; Davies, K.J.A.; Henze, A.; Grune, T. The molecular chaperone Hsp70 promotes the proteolytic removal of oxidatively damaged proteins by the proteasome. *Free Radic Biol Med.* **2016**, *99*, 153–166. [[CrossRef](#)] [[PubMed](#)]
44. Deshmukh, F.K.; Yaffe, D.; Olshina, M.A.; Ben-Nissan, G.; Sharon, M. The contribution of the 20S proteasome to proteostasis. *Biomolecules* **2020**, *9*, 190. [[CrossRef](#)]
45. Paesano, L.; Perotti, A.; Buschini, A.; Carubbi, C.; Marmiroli, M.; Maestri, E.; Iannotta, S.; Marmiroli, N. Markers for toxicity to HepG2 exposed to cadmium sulphide quantum dots; damage to mitochondria. *Toxicology* **2016**, *374*, 18–28. [[CrossRef](#)] [[PubMed](#)]
46. Go, Y.-M.; Roede, J.R.; Orr, M.; Liang, Y.; Jones, D.P. Integrated redox proteomics and metabolomics of mitochondria to identify mechanisms of Cd toxicity. *Toxicol. Sci.* **2014**, *139*, 59–73. [[CrossRef](#)] [[PubMed](#)]
47. Wang, T.; Wang, Q.; Song, R.; Zhang, Y.; Yang, J.; Wang, Y.; Yuan, Y.; Bian, J.; Liu, X.; Gu, J.; et al. Cadmium induced inhibition of autophagy is associated with microtubule disruption and mitochondrial dysfunction in primary rat cerebral cortical neurons. *Neurotoxicol. Teratol.* **2016**, *53*, 11–18. [[CrossRef](#)] [[PubMed](#)]
48. Wang, J.; Deng, W.; Zou, T.; Bai, B.; Chang, A.K.; Ying, X. Cadmium-induced oxidative stress in *Meretrix meretrix* gills leads to mitochondria-mediated apoptosis. *Ecotoxicology* **2021**, *30*, 2011–2023. [[CrossRef](#)]
49. Chen, G.; Wei, T.; Ju, F.; Li, H. Protein quality control and aggregation in the endoplasmic reticulum: From basic to bedside. *Front. Cell Dev. Biol.* **2023**, *11*, 1156152. [[CrossRef](#)]
50. Pham, K.; Pal, R.; Qu, Y.; Liu, X.; Yu, H.; Shiao, S.; Wand, X.; O'Brian Smith, E.; Cui, X.; Rodney, G.G.; et al. Nuclear glutaredoxin 3 is critical for protection against oxidative stress-induced cell death. *Free Radic. Biol. Med.* **2015**, *85*, 197–206. [[CrossRef](#)]

51. Bao, Y.; Liu, X.; Zhang, W.; Cao, J.; Li, W.; Li, C.; Lin, Z. Identification of a regulation network in response to cadmium toxicity using blood clam *Tegillarca granosa* as model. *Sci. Rep.* **2016**, *6*, 35704. [[CrossRef](#)] [[PubMed](#)]
52. Wu, H.; Xu, L.; Ji, C.; Yu, D. Proteomic and metabolomic responses in D-shape larval mussels *Mytilus galloprovincialis* exposed to cadmium and arsenic. *Fish Shellfish Immunol.* **2016**, *58*, 514–520. [[CrossRef](#)] [[PubMed](#)]
53. Granger Joly de Boissel, P.; Fournier, M.; Rodriguez-Lecompte, R.C.; McKenna, P.; Kibenge, F.; Siah, A. Functional and molecular responses of the blue mussel *Mytilus edulis* hemocytes exposed to cadmium—An in vitro model and transcriptomic approach. *Fish Shellfish Immunol.* **2017**, *67*, 575–585. [[CrossRef](#)] [[PubMed](#)]
54. Meng, J.; Wang, W.; Li, L.; Yin, Q.; Zhang, G. Cadmium effects on DNA and protein metabolism in oyster (*Crassostrea gigas*) revealed by proteomic analyses. *Sci. Rep.* **2017**, *7*, 11716. [[CrossRef](#)] [[PubMed](#)]
55. Company, R.; Antúnez, O.; Cosson, R.P.; Serafim, A.; Shillito, B.; Cajaraville, M.; Bebianno, M.J.; Torreblanca, A. Protein expression profiles in *Bathymodiolus azoricus* exposed to cadmium. *Ecotoxicol. Environ. Saf.* **2019**, *171*, 621–630. [[CrossRef](#)] [[PubMed](#)]
56. Ferreira, C.P.; Lima, D.; Paiva, R.; Vilke, J.M.; Mattos, J.J.; Almeida, E.A.; Grott, S.C.; Alves, T.C.; Corrêa, J.N.; Jorge, M.B.; et al. Metal bioaccumulation, oxidative stress and antioxidant responses in oysters *Crassostrea gasar* transplanted to an estuary in southern Brazil. *Sci. Total Environ.* **2019**, *685*, 332–344. [[CrossRef](#)] [[PubMed](#)]
57. Huang, J.; Wu, X.; Tian, F.; Chen, Q.; Luo, P.; Zhang, F.; Wan, X.; Zhong, Y.; Liu, Q.; Lin, T. Changes in proteome and protein phosphorylation reveal the protective roles of exogenous nitrogen in alleviating cadmium toxicity in poplar plants. *Int. J. Mol. Sci.* **2020**, *21*, 278. [[CrossRef](#)]
58. Lu, Z.; Wang, S.; Shan, X.; Ji, C.; Wu, H. Differential biological effects in two pedigrees of clam *Ruditapes philippinarum* exposed to cadmium using iTRAQ-based proteomics. *Environ. Toxicol. Pharmacol.* **2019**, *65*, 66–72. [[CrossRef](#)] [[PubMed](#)]
59. Rono, M.K.; Muturi, C.N.; Ochieng, R.; Mwakubabanya, R.; Wachira, F.N.; Mwangangi, J.; Kinyanjui, S.; Njunge, J.; Mireji, P.O. Cadmium tolerance pathway in *Anopheles gambiae* sensu stricto. *Acta Tropica* **2019**, *198*, 105033. [[CrossRef](#)]
60. Liu, H.; Tian, X.; Jiang, L.; Han, D.; Hu, S.; Cui, Y.; Jiang, F.; Liu, Y.; Xu, Y.; Li, H. Sources, bioaccumulation, and toxicity mechanisms of cadmium in *Chlamys farreri*. *J. Hazard. Mater.* **2023**, *453*, 131395. [[CrossRef](#)]
61. Cui, Y.; Freedman, J.H. Cadmium induces retinoic acid signaling by regulating retinoic acid metabolic gene expression. *J. Biol. Chem.* **2009**, *284*, 24925–24932. [[CrossRef](#)] [[PubMed](#)]
62. Luo, L.; Ke, C.; Guo, X.; Shi, B.; Huang, M. Metal accumulation and differentially expressed proteins in gill of oyster (*Crassostrea hongkongensis*) exposed to long-term heavy metal-contaminated estuary. *Fish Shellfish Immunol.* **2014**, *38*, 318–329. [[CrossRef](#)] [[PubMed](#)]
63. Zhang, Y.; Ali, A.; Jin, Z.; Pei, Y.; Yang, G. Induction of cystathionine gamma-lyase expression and metallothionein-1 S-sulfhydration alleviate cadmium-induced cell death in myoblast cells. *Ecotoxicol. Environ. Saf.* **2019**, *179*, 222–231. [[CrossRef](#)] [[PubMed](#)]
64. Dickhout, J.; Carlisle, R.E.; Jerome, D.E.; Mohammed-Ali, Z.; Jiang, H.; Yang, G.; Mani, S.; Garg, S.K.; Banerjee, R.; Kaufman, R.J.; et al. Integrated stress response modulates cellular redox state via induction of cystathionine γ -lyase: Cross-talk between integrated stress response and thiol metabolism. *J. Biol. Chem.* **2012**, *287*, 7603–7614. [[CrossRef](#)] [[PubMed](#)]
65. Marchione, R.; Leibovitch, S.A.; Lenormand, J.-L. The translational factor eIF3f: The ambivalent eIF3 subunit. *Cell. Mol. Life Sci.* **2013**, *70*, 3603–3616. [[CrossRef](#)] [[PubMed](#)]
66. Zhou, Z.; Lu, Q.; Huang, Q.; Zheng, C.; Chen, B.; Lei, Y. EIF3 regulates migration, invasion and apoptosis in cadmium transformed 16HBE cells and is a novel biomarker of cadmium exposure in a rat model and in workers. *Toxicol. Res.* **2016**, *5*, 761–772. [[CrossRef](#)] [[PubMed](#)]
67. Stevenson, B.; Gorman, M.A.; Koach, J.; Cheung, B.; Marshall, G.M.; Parker, M.W.; Holien, J.K. A structural view of PA2G4 isoforms with opposing functions in cancer. *J. Biol. Chem.* **2020**, *295*, 16100–16112. [[CrossRef](#)] [[PubMed](#)]
68. Martínez-Reyes, I.; Chandel, N.S. Mitochondrial TCA cycle metabolites control physiology and disease. *Nat. Commun.* **2020**, *11*, 102. [[CrossRef](#)] [[PubMed](#)]
69. Sokolova, I.M.; Sokolov, E.P.; Ponnappa, K.V. Cadmium exposure affects mitochondrial bioenergetics and gene expression of key mitochondrial proteins in the eastern oyster *Crassostrea virginica* Gmelin (Bivalvia: Ostreidae). *Aq. Toxicol.* **2005**, *73*, 242–255. [[CrossRef](#)]
70. Hanana, H.; Kleinert, C.; André, C.; Gagné, F. Influence of cadmium on oxidative stress and NADH oscillations in mussel mitochondria. *Comp. Biochem. Physiol. C* **2019**, *216*, 60–66. [[CrossRef](#)]
71. Ji, C.; Lu, Z.; Xu, L.; Li, F.; Cong, M.; Shan, X.; Wu, H. Evaluation of mitochondrial toxicity of cadmium in clam *Ruditapes philippinarum* using iTRAQ-based proteomics. *Environ. Pollut.* **2019**, *251*, 802–810. [[CrossRef](#)] [[PubMed](#)]
72. Zhang, R.; Zhu, H.; Yaun, Y.; Wang, Y.; Tian, Z. SPAG6 promotes cell proliferation and inhibits apoptosis through the PTEN/PI3K/AKT pathway in Burkitt lymphoma. *Oncol. Rep.* **2020**, *44*, 2021–2030. [[CrossRef](#)] [[PubMed](#)]
73. Dalle-Donne, I.; Rossi, R.; Milzani, A.; Di Simplicio, P.; Colombo, R. The actin cytoskeleton response to oxidants: From small heat shock protein phosphorylation to changes in the redox state of actin itself. *Free Radic. Biol. Med.* **2001**, *31*, 1624–1632. [[CrossRef](#)] [[PubMed](#)]
74. McDonagh, B.; Tyther, R.; Sheehan, D. Carbonylation and glutathionylation of proteins in the blue mussel *Mytilus edulis* detected by proteomic analysis and Western blotting: Actin as a target for oxidative stress. *Aquat. Toxicol.* **2005**, *73*, 315–326. [[CrossRef](#)] [[PubMed](#)]

75. Chora, S.; Starita-Geribaldi, M.; Guignonis, J.-M.; Samsom, M.; Roméo, M.; Bebianno, M.J. Effect of cadmium in the clam *Ruditapes decussatus* assessed by proteomic analysis. *Aquat. Toxicol.* **2009**, *94*, 300–308. [[CrossRef](#)] [[PubMed](#)]
76. Dailianis, S.; Patetsini, E.; Kaloyanni, M. The role of signalling molecules on actin glutathionylation and protein carbonylation induced by cadmium in haemocytes of mussel *Mytilus galloprovincialis* (Lmk). *J. Exp. Biol.* **2009**, *212*, 3612–3620. [[CrossRef](#)] [[PubMed](#)]
77. Liu, F.; Wang, D.-Z.; Wang, W.-X. Cadmium-induced changes in trace element bioaccumulation and proteomics perspective in four marine bivalves. *Environ. Toxicol. Chem.* **2012**, *31*, 1292–1300. [[CrossRef](#)] [[PubMed](#)]
78. Thompson, E.L.; Taylor, D.A.; Nair, S.V.; Birch, G.; Haynes, P.A.; Raftos, D.A. Proteomic discovery of biomarkers of metal contamination in Sydney Rock oysters (*Saccostrea glomerata*). *Aq. Toxicol.* **2012**, *109*, 202–212. [[CrossRef](#)] [[PubMed](#)]
79. Melwani, A.R.; Thompson, E.L.; Raftos, D.A. Differential proteomic response of Sydney rock oysters (*Saccostrea glomerata*) to prolonged environmental stress. *Aquat. Toxicol.* **2016**, *173*, 53–62. [[CrossRef](#)]
80. Liu, Y.; Xiao, W.; Shinde, M.; Field, J.; Templeton, D.M. Cadmium favors F-actin depolymerization in rat renal mesangial cells by site-specific, disulfide-based dimerization of the CAP1 protein. *Arch. Toxicol.* **2018**, *92*, 1049–1064. [[CrossRef](#)]
81. Pizzazia, D.; Nogueira, M.L.; Mondin, M.; Carvalho, M.E.A.; Piotto, F.A.; Rosario, M.F.; Azevedo, R.A. Cadmium toxicity and its relationship with disturbances in the cytoskeleton, cell cycle and chromosome stability. *Ecotoxicology* **2019**, *28*, 1046–1055. [[CrossRef](#)] [[PubMed](#)]
82. Perlson, E.; Medzihradsky, K.F.; Darula, Z.; Munno, D.W.; Syed, N.I.; Burlingame, A.L.; Fainzilber, M. Differential proteomics reveals multiple components in retrogradely transported axoplasm after nerve injury. *Mol. Cell Proteom.* **2004**, *3*, 510–520. [[CrossRef](#)] [[PubMed](#)]
83. Frascotti, G.; Galbiati, E.; Mazzucchelli, M.; Pozzi, M.; Salvioni, L.; Vertemara, J.; Tortora, P. The Vault nanoparticle: A gigantic ribonucleoprotein assembly involved in diverse physiological and pathological phenomena and an Ideal nanovector for drug delivery and therapy. *Cancers* **2021**, *13*, 707. [[CrossRef](#)] [[PubMed](#)]
84. Grossi, S.; Fenini, G.; Kockmann, T.; Hennig, P.; Di Filippo, M.; Beer, H.D. Inactivation of the cytoprotective major vault protein by caspase-1 and -9 in epithelial cells during apoptosis. *J. Investig. Dermatol.* **2020**, *140*, 1335–1345.e10. [[CrossRef](#)] [[PubMed](#)]
85. Goswami, P.; Hariharan, G.; Godhantaraman, N.; Munuswamy, N. An integrated use of multiple biomarkers to investigate the individual and combined effect of copper and cadmium on the marine green mussel (*Perna viridis*). *J. Environ. Sci. Health A* **2014**, *49*, 1564–1577. [[CrossRef](#)] [[PubMed](#)]
86. Dixit, U.; Liu, Z.; Pandey, A.K.; Kothari, R.; Pandey, V.N. Fuse binding protein antagonizes the transcription activity of tumor suppressor protein p53. *BMC Cancer* **2014**, *14*, 925. [[CrossRef](#)]
87. Jang, M.; Park, B.C.; Kang, S.; Chi, S.-W.; Cho, S.; Chung, S.J.; Lee, S.C.; Bae, K.-H.; Park, S.G. Far upstream element-binding protein-1, a novel caspase substrate, acts as a cross-talker between apoptosis and the c-myc oncogene. *Oncogene* **2009**, *12*, 1529–1536. [[CrossRef](#)]
88. Zhao, D.; Hu, G.; Chen, R.; Xiao, G.; Teng, S. Molecular cloning, characterization, and tissue distribution of c-Myc from blood clam *Tegillarca granosa* and its role in cadmium-induced stress response. *Gene* **2022**, *834*, 14661. [[CrossRef](#)]
89. Shih, J.-W.; Wang, W.-T.; Tsai, T.-Y.; Kuo, C.-Y.; Li, H.-K.; Wu Lee, Y.-H. Critical roles of RNA helicase DDX3 and its interactions with eIF4E/PABP1 in stress granule assembly and stress response. *Biochem. J.* **2012**, *441*, 119–129. [[CrossRef](#)]
90. Princely Abudu, Y.; Pankiv, S.; Mathai, B.J.; Håkon Lystad, A.; Bindesbøll, C.; Brenne, H.B.; Yoke Wui Ng, M.; Thiede, B.; Yamamoto, A.; Mutugi Nthiga, T.; et al. NIPSNAP1 and NIPSNAP2 Act as “Eat Me” Signals for Mitophagy. *Dev. Cell* **2019**, *49*, 509–525.e12. [[CrossRef](#)]
91. Dan, X.; Babbar, M.; Moore, A.; Wechter, N.; Tian, J.; Mohanty, J.G.; Croteau, D.L.; Bohr, V.A. DNA damage invokes mitophagy through a pathway involving Spata18. *Nucleic Acids Res.* **2020**, *48*, 6611–6623. [[CrossRef](#)] [[PubMed](#)]
92. Wakasugi, K.; Yokosawa, T. Chapter Eight-Non-canonical functions of human cytoplasmic tyrosyl-, tryptophanyl- and other aminoacyl-tRNA synthetases. *Enzymes* **2020**, *48*, 207–242. [[CrossRef](#)] [[PubMed](#)]
93. Sun, Z.; Yang, C.; Wang, L.; Wang, X.; Wang, J.; Yue, F.; Liu, R.; Zhang, H.; Song, L. The protein expression profile in hepatopancreas of scallop *Chlamys farreri* under heat stress and *Vibrio anguillarum* challenge. *Fish Shellfish Immunol.* **2014**, *36*, 252–260. [[CrossRef](#)]
94. Zhang, Z.; Miao, L.; Xin, X.; Zhang, J.; Yang, S.; Miao, M.; Kong, X.; Jia, B. Underexpressed CNDP2 participates in gastric cancer growth inhibition through activating the MAPK signaling pathway. *Mol. Med.* **2014**, *20*, 17–28. [[CrossRef](#)]
95. van Vliet, A.R.; Giordano, F.; Gerlo, S.; Segura, I.; Van Eygen, S.; Molenberghs, G.; Rocha, S.; Houcine, A.; Derua, R.; Verfaillie, T.; et al. The ER Stress Sensor PERK Coordinates ER-Plasma Membrane Contact Site Formation through Interaction with Filamin-A and F-Actin Remodeling. *Mol. Cell* **2017**, *65*, 885–899.e6. [[CrossRef](#)]
96. Lewinska, A.; Klukowska-Rötzler, J.; Deregowskad, A.; Adamczyk-Grochalaa, J.; Wnuk, M. c-Myc activation promotes cofilin-mediated remodeling and telomere homeostasis as a response to oxidant-based DNA damage in medulloblastoma cells. *Redox Biol.* **2019**, *24*, 101163. [[CrossRef](#)]
97. Devin, S.; Potet, M.; Louis, F.; Pauly, D.; Rocher, B.; Wagner, P.; Giambérini, L.; Pain-Devin, S. Spatial and seasonal use of biomarkers in dreissenids: Implications for biomonitoring. *Environ. Sci. Pollut. Res.* **2023**. [[CrossRef](#)]
98. Potet, M.; Giambérini, L.; Pain-Devin, S.; Louis, F.; Bertrand, C.; Devin, S. Differential tolerance to nickel between *Dreissena polymorpha* and *Dreissena rostriformis bugensis* populations. *Sci. Rep.* **2018**, *8*, 700. [[CrossRef](#)] [[PubMed](#)]
99. Wang, Q.; Zhu, J.; Zhang, K.; Jiang, C.; Wang, Y.; Yuan, Y.; Bian, J.; Liu, X.; Gu, J.; Liu, Z. Induction of cytoprotective autophagy in PC-12 cells by cadmium. *Biochem. Biophys. Res. Commun.* **2013**, *438*, 186–192. [[CrossRef](#)]

100. Quinta, H.R.; Galigniana, N.M.; Erlejman, A.G.; Lagadari, M.; Piwien-Pilipuk, G.; Galigniana, M.D. Management of cytoskeleton architecture by molecular chaperones and immunophilins. *Cell. Signal.* **2011**, *23*, 1907–1920. [[CrossRef](#)]
101. Kung, C.-P.; Wu, Y.-R.; Chuang, H.-W. Expression of a dye-decolorizing peroxidase results in hypersensitive response to cadmium stress through reducing the ROS signal in Arabidopsis. *Environ. Exp. Bot.* **2014**, *101*, 47–55. [[CrossRef](#)]
102. Antonioli, M.; Albiero, F.; Piacentini, M.; Fimia, G.M. Temporal regulation of autophagy response by the CULLIN 4-AMBRA1-CULLIN 5 axis. *Mol. Cell Oncol.* **2015**, *3*, e10083042016. [[CrossRef](#)]
103. Díaz-Ramos, À.; Roig-Borrellas, A.; García-Melero, A.; López-Aleman, R. α -Enolase, a Multifunctional Protein: Its Role on Pathophysiological Situations. *J. Biomed. Biotechnol.* **2012**, *2012*, 1567952012. [[CrossRef](#)]
104. Zandberg, L.; van Dyk, H.C.; van der Westhuizen, F.H.; van Dijk, A.A. A 3-methylcrotonyl-CoA carboxylase deficient human skin fibroblast transcriptome reveals underlying mitochondrial dysfunction and oxidative stress. *Int. J. Biochem. Cell Biol.* **2016**, *78*, 116–129. [[CrossRef](#)]
105. Zhang, H.-L.; Liu, Z.-H.; Luo, Q.; Wang, Y.; Zhao, Z.-H. Abnormal expression of NSF, α -SNAP and SNAP23 in pulmonary arterial hypertension in rats treated with monocrotaline. *Int. J. Clin. Exp. Med.* **2015**, *8*, 1834–1843.
106. Muralidharan, S.; Thompson, E.; Raftos, D.; Birch, G.; Haynes, P.A. Quantitative proteomics of heavy metal stress responses in Sydney rock oysters. *Proteomics* **2012**, *12*, 906–921. [[CrossRef](#)]
107. Latorre-Muro, P.; Baeza, J.; Armstrong, E.; Hurtado-Guerrero, R.; Corzana, F.; Wu, L.; Sinclair, D.A.; Lopez-Buesa, P.; Carrodegua, J.A.; Denu, J.M. Dynamic acetylation of phosphoenolpyruvate carboxykinase toggles enzyme activity between gluconeogenic and anaplerotic reactions. *Mol. Cell* **2018**, *71*, 718–732. [[CrossRef](#)] [[PubMed](#)]
108. Mori, C.; Lee, J.-Y.; Tokumoto, M.; Satoh, M. Cadmium toxicity is Regulated by peroxisome proliferator-activated receptor δ in human proximal tubular cells. *Int. J. Mol. Sci.* **2022**, *23*, 8652. [[CrossRef](#)] [[PubMed](#)]
109. Muthukumar, K.; Nachiappan, V. Phosphatidylethanolamine from phosphatidylserine decarboxylase2 is essential for autophagy under cadmium stress in *Saccharomyces cerevisiae*. *Cell Biochem. Biophys.* **2013**, *67*, 1353–1363. [[CrossRef](#)]
110. Adle, D.J.; Wei, W.; Smith, N.; Bies, J.J.; Lee, J. Cadmium-mediated rescue from ER-associated degradation induces expression of its exporter. *Proc. Natl. Acad. Sci. USA* **2008**, *106*, 10189–10194. [[CrossRef](#)]
111. Song, C.; Xiao, Z.; Nagashima, K.; Li, C.-C.H.; Lockett, S.J.; Dai, R.-M.; Cho, E.H.; Conrads, T.P.; Veenstra, T.D.; Colburn, N.H.; et al. The heavy metal cadmium induces valosin-containing protein (VCP)-mediated aggresome formation. *Toxicol. Appl. Pharmacol.* **2008**, *228*, 351–363. [[CrossRef](#)] [[PubMed](#)]
112. Pennington, K.L.; Chan, T.Y.; Torres, M.P.; Andersen, J.L. The dynamic and stress-adaptive signaling hub of 14-3-3: Emerging mechanisms of regulation and context-dependent protein–protein interactions. *Oncogene* **2018**, *37*, 5587–5604. [[CrossRef](#)] [[PubMed](#)]

Disclaimer/Publisher’s Note: The statements, opinions and data contained in all publications are solely those of the individual author(s) and contributor(s) and not of MDPI and/or the editor(s). MDPI and/or the editor(s) disclaim responsibility for any injury to people or property resulting from any ideas, methods, instructions or products referred to in the content.